MASTER'S THESIS
60 ECTS

Measurements of total air content of ice from EUROCORE, Greenland

Johanne Aagaard

Centre for Ice and Climate
Niels Bohr Institute
Faculty of Science
University of Copenhagen

Supervisors:
Thomas Blunier & Bo M. Vinther
Centre for Ice and Climate, University of Copenhagen

Submitted: 6st January 2015

Abstract

Total air content in ice sheets is directly related to the elevation of the ice sheet surface at the time the air is enclosed in the ice. This is one of the only ways to determine the elevation of the ice sheets in the past, making the study of total air content of the ice important.

This thesis is an attempt to further develop and improve an apparatus to measure total air content build by Sebastian Bender (2012). The apparatus is based on the barometric method described by Lipenkov et al. (1995). The basic idea in the experiment is to extract the trapped air from an ice sample by melting and refreezing the ice under vacuum in a known volume, and measuring the pressure and temperature.

In the earlier experiment not all air was extracted from the ice. Therefore the apparatus was expanded with an air trap (a filter with HayeSep polymers). With this expansion it is possible to perform several melting/refreezing cycles and trap the air between cycles. It is concluded that only two cycles are necessary to extract all air from the ice sample.

The extraction chamber is no longer a part of the measuring area which has some advantages: a temperature gradient is no longer present in the measuring area, the volume of this area no longer changes due to volume change of the ice samples, and the duration of the experiment is shortened. A water trap, installed just before the air trap to dry the air before entrapment, should decrease the water vapor pressure to be neglectable, but it is not working optimally, resulting in a small indeterminable error.

11 samples from EUROCORE, Greenland, are measures. The total air content is corrected for the error of the bubbles that are cut on the surface of the sample, which is found to be 5.42%. The total air content results lie between $0.0835 - 0.0922 \frac{\text{cm}^3}{\text{g}}$ and have a mean value of $0.0881 \frac{\text{cm}^3}{\text{g}}$. The error of the measurements is 2.18%. The results of the total air content are close to results obtained in other studies from the same site. The results also show seasonal variations that fit the variations of the $\delta^{18}O$ record from the same depth.

It is concluded that the experiment is working. The expansion with an air trap is successful and the obtained results of the total air content are good though they are a little low.

Resumé

Det totale luftindhold i iskapper er direkte relateret til højden af iskappens over-flade på det tidspunkt, hvor luften er lukket inde i isen. Dette er en af de eneste metoder til at bestemme elevationen af en iskappe tilbage i tiden, hvilket gør studiet af det totale luftindhold i isen vigtigt.

I dette speciale videreudvikles et apparat til at måle det totale luftindhold, som tidligere er bygget af Bender (2012). Apparatet er baseret på en barometrisk metode beskrevet af Lipenkov et al. (1995). Ideen i eksperimentet er at trække luften ud af en isprøve ved at smelte og genfryse den under vakuum i en kendt volumen, og måle tryk og temperatur.

I det tidligere eksperiment var, blev ikke alt luften trukket ud af isen. Derfor blev apparatet udvidet med en luftfælde (et filter med HayeSep polymerer). Med denne udvidelse er det muligt at udføre flere smeltnings- og genfrysningscykler. Det konkluderes, at kun to cykler er nødvendige for at trække alt luften ud af isprøven.

Kammeret med isprøven er ikke længere en del af målingsområdet, hvilket har nogle fordele: der er ikke længere en temperaturgradient til stede i måleområdet, volumen af måleområdet ændres ikke længere på grund af ændring af isprøvens volumen, og varigheden af eksperimentet er blevet forkortet. En vanddampfælde, som er installeret lige før luftfælden for at tørre luften før den fanges, burde formindske vanddamptrykket, så det kan negligeres, men denne virker ikke optimalt, hvilket resulterer i lille en ubestemmelig fejl.

Der er målt på 11 isprøver fra EUROCORE, Grønland. Det totale luftindhold korrigeres for den fejl, der er fordi boblerne på overfladen af prøven er skåret over. Denne er fundet til at være 5.42%. Det målte totale luftindhold ligger mellem $0.0835 - 0.0922\frac{\text{cm}^3}{\text{g}}$ og har en middelværdi på $0.0881\frac{\text{cm}^3}{\text{g}}$. Fejlen for målingerne er 2.18%. Resultaterne af det totale luftindhold er tæt på resutalter opnået af andre studier fra samme sted, men de er lidt lave. Resultaterne viser også årsvariationer som passer med de variationer der ses på $\delta^{18}O$ målinger fra samme dybde.

Det konkluderes at eksperimentet virker. Udbyggelsen med en luftfælde er succesfuld og de opnåede resultater af det totale luftindhold er lidt lave, men gode.

Preface

This thesis represents the completion of my master's degree in physics with qualification profile in geophysics, conducted in the period 2012-2015 at the Niels Bohr Institute, University of Copenhagen. The thesis was carried out in the time frame of 1 year, corresponding to 60 ECTS point, at the Centre for Ice and Climate under the supervision of Thomas Blunier and Bo M. Vinther.

Johanne Aagaard
University: University of Copenhagen
Institute: Niels Bohr Institute
Department: Centre for Ice and Climate
Author: Johanne Aagaard
Email: jo_aa_77@hotmail.com
KU-username: vcp281
Study title: Measurements of total air content of ice from EUROCORE, Greenland
Academic advisor: Thomas Blunier and Bo M. Vinther, Centre for Ice and Climate.
Submitted: January 6st, 2015.

Contents

Chapter 1

Introduction

The study of ice sheets has for many years been utilized as a source of information about the past climate. Ice sheets are dynamic systems influenced by the climate of the Earth. They are very sensitive to climate changes, since changes in temperature and precipitation alter the mass balance of the ice sheets. At the same time ice sheets influence the climate by changing the albedo, atmospheric temperature and affecting the hydrological system on the Earth by influencing the temperature, salinity and sea level of the oceans [Cuffey and Paterson, 2010].

The alternation between glacial and interglacial periods are affected by the Milankovitch forcings: changes in the solar insolation induced by the Earth's position relative to the sun. These cycles of 19,000 and 23,000, 41,000 and 100,000 years due to precession of the Earth's axis of rotation, obliquity and eccentricity of the Earth's orbit, respectively, appear in ice-volume records [Cuffey and Paterson, 2010].

Studying ice sheets is important to understand their dynamics and the interaction between ice sheets and the climate system. Especially in a time where global warming is an important issue this is very relevant. The big ice sheets in Greenland and Antarctica contain unique records of the changes of the Earth's climate such as temperature and accumulation as well as chemical compounds from the atmosphere. The ice sheets consist of annual layers. These layers contain information about many parameters of the Earth's climate. They are investigated from drilled ice cores from the ice sheets, which is an important part of testing climate models and their ability to reproduce the climate in the past.

Since the mass balance changes with climate the size of the ice sheets is always changing. Today glaciers[1] cover around 10% of the land surface of the Earth. There has been periods in the Earth's history where the ice has been completely gone, while during ice ages ice sheets have covered three times as much as they

---

[1]Glaciers include both the big ice sheets in Greenland and Antarctica, smaller ice caps and local glaciers.

do today [Cuffey and Paterson, 2010]. When the ice sheets grow or shrink the thickness of the ice sheets also changes. Thus the elevation of the surface changes continuously. However the knowledge of the surface elevation of ice sheets through time is limited. Ice sheet models can be used to model the elevation, but generally they underestimate the extend and elevation of the ice sheet [Vinther et al., 2009]. It is essential to be able to verify the model results by comparing them to measured results. The total air content in the ice sheets is a way to determine the surface elevation, since the air content depends on the air pressure and thus the elevation of the glacier [Raynaud et al., 2007, Vinther et al., 2009]. This makes the study of total air content of glacial ice important.

1.1   Transformation from snow to ice

Snow is transformed to ice through processes of sintering and packing of the snow grains [Martinerie et al., 1992]. The intermediate state of transformation between snow and ice is called firn. The transition between snow and firn is smooth because the physical properties do not change abruptly, and it can therefore be difficult to distinguish. The transformation between firn and ice is clearly defined as the pore close-off, which refers to the process where the air filled pores between the grains are sealed [Cuffey and Paterson, 2010]. At the close-off the pores are sealed off and the air is now present as isolated bubbles in the ice. Figure 1.1 show the transformation from snow to ice. In the melting free zones of the polar ice sheets this process occurs in the first 50-120 m below the surface [Raynaud et al., 1997].

The amount of air trapped in the ice, the total air content denoted V, is a measure of volume of dry air per mass of ice and is usually expressed in $\frac{\text{cm}^3\text{STP}}{\text{g of ice}}$, where STP is the standard conditions of the temperature (273 K) and the pressure (1013hPa) [Lipenkov et al. 1995].
The total air content depends on the pore volume V_c (expressed as $\frac{\text{cm}^3}{\text{g}}$), the atmospheric pressure P_c and the temperature T_c prevailing at the close-off. The total air content, V, can be calculated as

$$V = V_c \frac{P_c T_0}{T_c P_0} \tag{1.1}$$

where P_0 is the standard pressure ($P_0 = 1013$hPa) and T_0 is the standard temperature ($T_0 = 273$K) [Lipenkov et al. 1995].
Since the air content depends on the atmospheric pressure it can be used as a proxy for the changes in the surface elevation of the ice sheet, since the air pressure decreases with height.
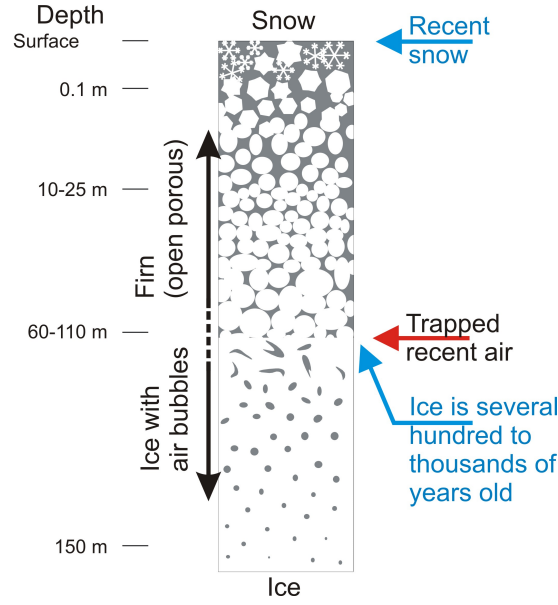
Figure 1.1: Illustration of the transformation from snow to firn (open pores), and then ice (isolated air bubbles). The red arrow show the depth of the close-off. Figure from personal communication with Thomas Blunier.

1.2 The total air content and elevation

Studies of the total air content and its relation to surface elevation was first presented in the 1970's. Raynaud and Lorius (1973) present measurements of the total air content from Camp Century in Greenland and show a decrease in the air content of 12.5% from 1000-1200 m depth. These depths correspond to the end of the last glacial. This increase in total air content suggest a significant increase in the ice sheet thickness during the last glaciation [Raynaud and Lorius, 1973]. Raynaud and Lebel (1979) did measurements of the total air content from six different sites with different temperature and elevation. The mean value from the different sites correlate linearly with the regression

$$V = -1.66 \cdot 10^{-5} E + 0.138 \qquad (1.2)$$

where E (m) is the elevation. The regression has a correlation coefficient of -0.998 [Raynaud and Lebel, 1979].
Martinerie et al. (1992) have compared measurements of the total air content from 16 different drill sites with the elevation of the air isolation depth E_i (m), and finds a clear relation between the air content and the elevation. Two of the sites (Camp Century and Mount Logan in Canada) are in the Northern Hemisphere, and the other 14 sites are in Antarctica. Five of the sites (BHJ, BHF, BHP, BHB and

BHQ) are located at low elevation on Low Dome, Antarctica where significant summer melt occurs. This means that refrozen melt layers are present, which affects the air content.

The $V - E_i$ relationship found by Martinerie et al. (1992) has a linear tendency however it is not completely linear. However, if the five sites with summer melt are not taken into account the following linear regression line, with high correlation coefficient (0.99), can be obtained for the Antarctica sites.

$$V = -1.68 \cdot 10^{-5} E_i + 0.141. \tag{1.3}$$

This is almost similar to the linear regression obtained by Raynaud and Lebel (1979).

Delmotte et al. (1999) present a plot with the measurements from the sites without summer melt from Martinerie et al. (1992) and results from Martinerie et al. (1994). Results from Raynaud et al. (1997) from GReenland Ice core Project (GRIP) and their own results from Dome Summit South (DSS) core from Law Dome in East Antarctica are added in the plot (see Figure 1.2). Furthermore newer
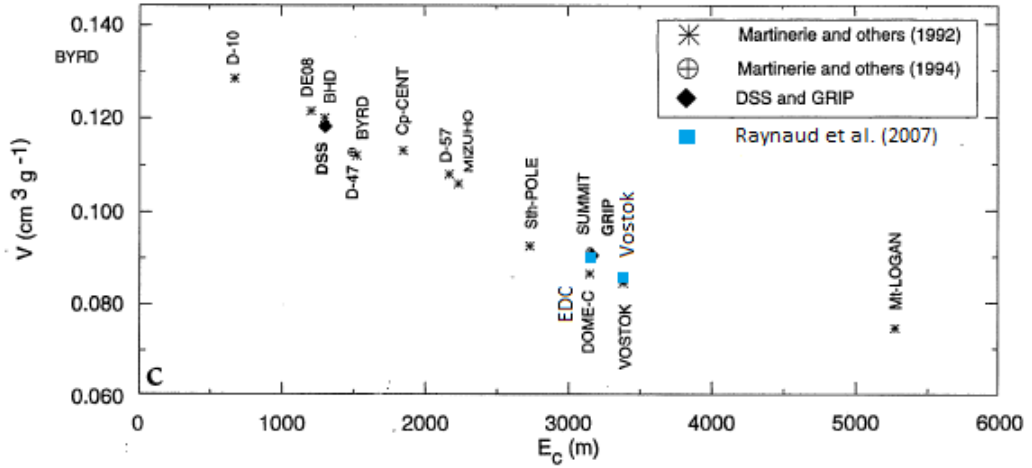
Figure 1.2: Air content versus elevation at close-off E_c. Crosses are adapted from Martinerie et al. (1992) and circles from Martinerie et al. (1994). The diamonds correspond to GRIP (Raynaud et al., 1997) and DSS from Delmotte et al., 1999, which are added by [Delmotte et al., 1999]. Blue squares correspond to results from two sites presented in Raynaud et al., 2007 from EDC (their own) and Vostok from Lipenkov et al., 1997. Figure modified from Delmotte et al. (1999).

results from Raynaud et al. (2007) at Dome C (EDC) and results from Lipenkov et al. (1997) from Vostok, Antarctica, are added in the plot [Raynaud et al., 2007].

Records of $\delta^{18}O$ from the ice are usually used as a proxy for past temperatures. Vinther et al. (2009) suggest that Greenland $\delta^{18}O$ records can also be used to estimate a change in elevation by comparing with $\delta^{18}O$ records from small marginal icecaps, where the ice sheet thickness is believed to be constant during most of the Holocene. $\delta^{18}O$ records from the last 12.000 years from six different drill sites from Greenland are presented in Figure 1.3b. Figure 1.3a show the locations of the six drill sites and their elevations. The trends in the $\delta^{18}O$ records seem to be similar in pairs related to their elevation: GRIP and NGRIP from the centre of the ice sheet, DYE-3 and Camp Century closer to the margins and Renland and Agassiz, which are small icecaps close to the Greenland Ice Sheet on opposite sides of Greenland. The ice thickness of the small ice caps on Renland and Agassiz do not change during the Holocene, and they are therefore used to estimate the elevation histories at the four Greenland sites from the changes in differences between the $\delta^{18}O$ records. In Figure 1.3c modeled the change in depositional elevation for GRIP and Camp Century are plotted together with total gas content measurements from both sites.
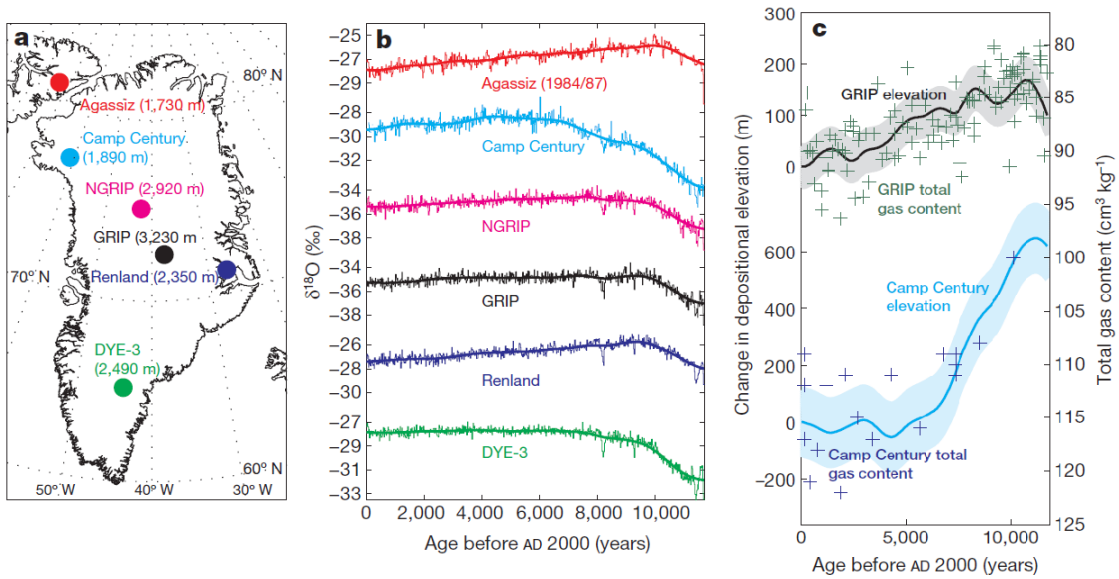
Figure 1.3: **a**: Location of the six drill sites in Greenland and Canada. Elevations are given in paranthesis. **b**: 20-year average and millennial scale trend of $\delta^{18}O$ during the Holocene as observed in ice core records from the six locations. All $\delta^{18}O$ values are expressed with respect to Vienna standard mean ocean water (V-SMOW). **c**: Modeled change in depositional elevation at the GRIP and Camp Century drill sites derived from water isotope differences compared with total gas measurements performed on the two ice cores. From [Vinther et al., 2009].

There are some uncertainties associated with using the total air content as a proxy for the past elevation of the ice sheet surface. The atmospheric pressure at a given location is not constant and can change on long-term scales due to changes in climate, which will influence P_c along with surface elevation. Furthermore the pore volume at close-off is not well known [Martinerie et al., 1992].

1.3   Other influencing parameters

Raynaud et al., 1997, presented results of the total air content from the GRIP core measured on ice that is up to 40,000 years old. These are seen in Figure
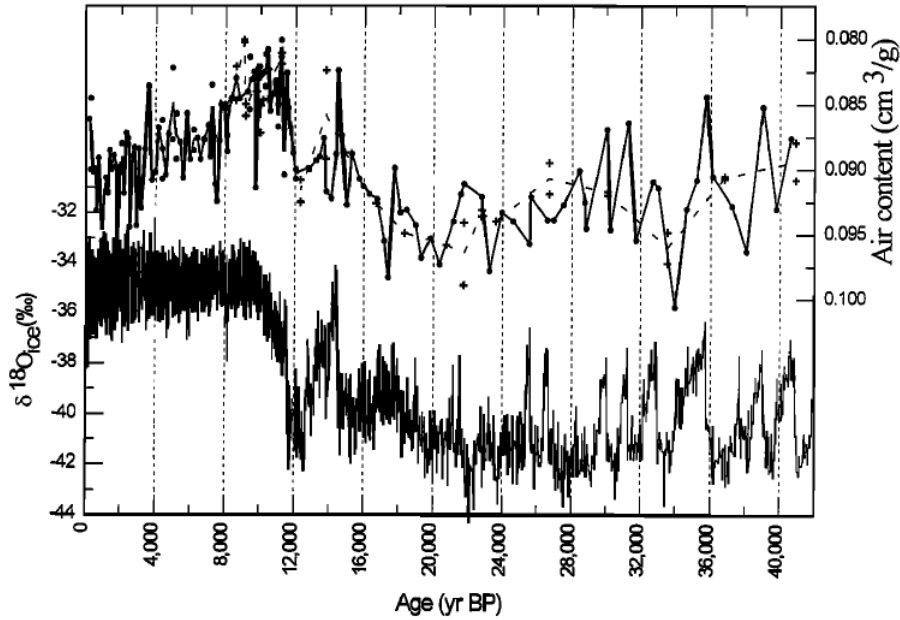
Figure 1.4: Record of GRIP air content (V) as a function of age for the last 40,000 years. Results were obtained by two different methods; a chromatographic measuring (dots and solid line) and a barometric measurement (crosses and dotted line). The lines run through the average at each depth level. The $\delta^{18}O$ record is also plotted for comparison. The two records can be directly compared, since the age difference between the trapped air and the ice has been taken into account. From [Raynaud et al., 1997].

1.4, where total air content is plotted as a function of age. The total air content was obtained by two different measuring methods; one using chromatographic measuring of the air peak (dots and solid line), and a barometric measurement of

the air in a calibrated volume (crosses and dotted line). The climatic ice isotopic record, $\delta^{18}O$, is also plotted versus age below the total air content.

These results show a clear change in the total air content between the Holocene (the last 11,000 years) and the Last Glacial Maximum. The long-term total air content trend shows a decrease of $\sim 13\%$ from the early Holocene to the Last Glacial Maximum. This long-term change can not be explained only by changes in the pressure and the temperature due to atmospheric changes, which suggests a change in the surface elevation. However, even changes in the elevation do not seem to be able to explain the big decrease, indicating that the porosity at close-off has an important influence on the total air content as well. The porosity at close-off is influenced by several atmospheric parameters. Wind speed can effect the snow packing and thereby the porosity but studies show that the wind speed need to exceed $6\frac{m}{s}$ to be able to influence the density and thereby the porosity [Raynaud et al., 2007, Martinerie et al., 1994].

Insolation can also have an influence on the porosity. The summer insolation is assumed to affect the rapid grain growth in the first meters of the snow by way of the temperature gradient during summer. This influence the porosity at close-off since the grain size has a direct impact on the densification process. The porosity at close-off would decrease with more intense insolation since the density at close-off increase with insolation. Thus the pore volume, and thereby the total air content, will decrease when insolation increases [Raynaud et al., 2007]. This
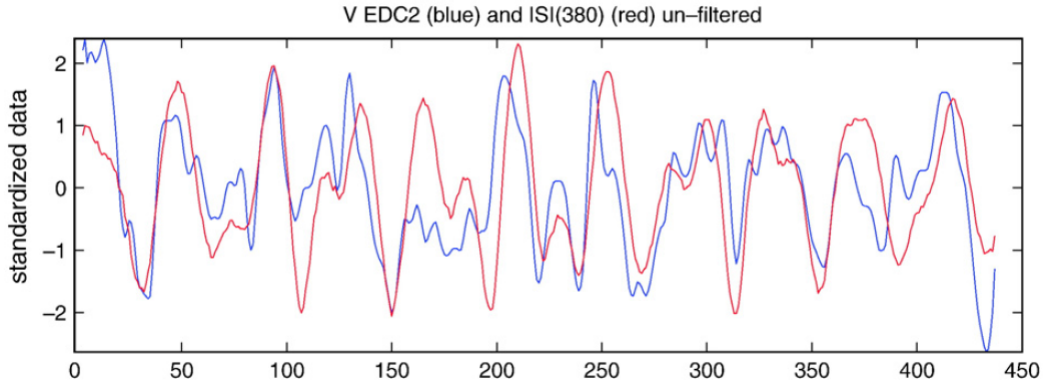
Figure 1.5: Normalised time series of ISI (red, $w_{threshold} = 380\frac{W}{m^2}$) and inversed V (blue, 2 points running window). From [Raynaud et al., 2007]

effect is seen in Figure 1.5, where the total air content, V, from EPICA DC (EDC) ice core from Antarctica and the integrated summer insolation (ISI (J)) are shown against age. ISI is obtained by summing the daily insolation, w_i $(\frac{W}{m^2})$ over the

year:

$$ISI = \sum \beta_i(w_i \cdot 86,400) \qquad (1.4)$$

where $\beta_i = 1$ when $w_i \geq w_{thresshold}$ and $\beta_i = 0$ otherwise, and $w_{threshold}$ is equal to about $380\frac{W}{m^2}$. In the obliquity and precession bands of the two signals are in good agreement.

Due to changes in temperature and accumulation the porosity also vary seasonally [Raynaud et al., 1997]. This seasonal change is seen in Figure 1.6, where measurements of air content from Law Dome in Antarctica is plotted versus depth. A plot of $\delta^{18}O$ from the same depth is plotted for comparison. This seasonal variation in air content occurs because the porosity in the summer layer is larger than that of the winter layer [Krinner et al. 2000]. The density of the winter layers is higher than the density of the summer layers due to higher accumulation. This might result in an isolation of the summer layer before its close-off if the pores in the denser winter layer is sealed off before the close-off of the summer layer [Delmotte et al., 1999].
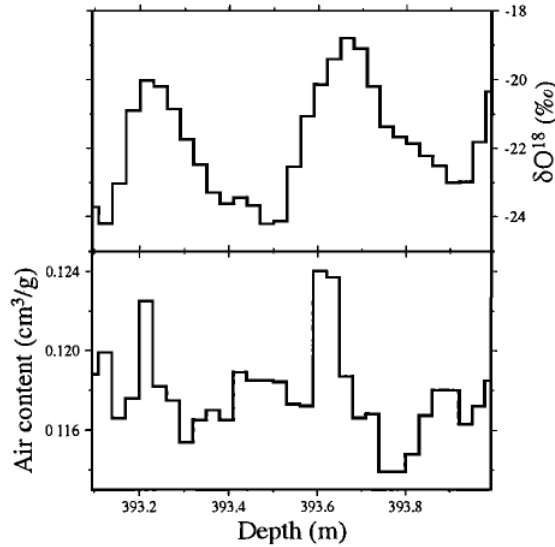
Figure 1.6: Time series of the observed air content and $\delta^{18}O$ at Law Dome in Antarctica. From [Krinner et al. 2000].

Different studies of the total air content have been made from both Greenland, Antarctica and from smaller glaciers in mountains [Delmotte et al., 1999, Krinner et al. 2000, Raynaud et al., 1997, Lipenkov et al. 1995]. Most of them show both long-term changes, which they claim are due to change in elevation and short-term, seasonal variation, due to changes in the porosity and the density.

The studies use different measuring techniques to determine the air content. One method is based on measuring the volume of the air in a burette[2] after extracting the air by melting the ice under a liquid. Another method extracts the air by melting and refreezing the ice and measuring the air peaks gas chromatographic. A vacuum volumetric technique measures the air volume in a burette after melting and refreezing under vacuum. A fourth method is a barometric method, where the air is extracted by crushing the ice in a known volume in vacuum. [Lipenkov et al. 1995].

1.4 Content of this thesis

This thesis is experimental and is an attempt to further develop and improve an apparatus to measure total air content build by Sebastian Bender (2012), a previous master student at Centre for Ice and Climate. The apparatus build by Bender (2012) is based on the barometric method described by Lipenkov et al. (1995). The basic idea in the experiment is to extract the trapped air bubbles from a sample by melting and refreezing the ice under vacuum in a known volume and measuring the pressure and temperature.

A major problem with the earlier experiment was that not all air was extracted from the ice in the first melting and refreezing cycle. Therefore the apparatus was expanded with an air trap with HayeSep, that is able to trap all the air between melting/refreezing cycles, so several cycles can be performed.

In this thesis 11 samples from the GRIP core from 280 m depth beneath the surface are measured.

Chapter 2 introduces the calculations that are used to find the total air content and presents the ice samples and their origin.
Chapter 3 describes the experimental setup and the changes and expansions of the setup, and outlines the experimental procedure.
Chapter 4 describes pressure gauge and volume calibrations.
Chapter 5 presents information about the ice samples from EUROCORE, and the cut bubble effect is determined.
Chapter 6 presents the results of the total air content of the ice samples from EUROCORE.
Chapter 7 discusses advantages and disadvantages of the new experimental setup, as well as the results and compare them to results from other studies and suggests further work.
Chapter 8 summarizes the conclusions.

---

[2]A volumetric burette is a device that measures volumes of liquids and gases.

Chapter 2

Calculating total air content

The ice samples that are measured in this thesis are from EROCORE ice core. In this chapter information about EUROCORE is presented. From this information and theoretical equations an expected total air content for the site can be calculated. Afterwards the equations, that are used to calculate the total air content from the parameters that are obtained in the experiment, are presented.

2.1 An estimate of total air content

From theoretical equations an estimate of the total air content expected at present at a certain site can be calculated from present day parameters. To be able to calculate an expected value of the total air content information about the drill site of the ice core is necessary. Therefore the drill site of the 11 samples measured in this thesis is described here.

2.1.1 EUROCORE

The samples are taken from the EUROCORE ice core drilled at 72.58°N and 37.54°W. EUROCORE is a shallow ice core drilled about 50 m from the deep ice core, GRIP, from Summit in central Greenland. This is the highest point of the Greenland Ice Sheet. In Figure 2.1 the GRIP drill site (among other drill sites in Greenland) is seen. The elevation at EUROCORE is 3240 m and the mean annual temperature is -32°C (=241K) [Haan et al., 1996]. Since EUROCORE and GRIP are only 50 m apart the conditions for the two cores are similar. At GRIP the close-off temperature and pressure are $T_c = 241.5$K and $P_c = 660 - 670$ mbar [Raynaud et al., 1997] and the present close-off depth is 71m [Schwander et al., 1997].
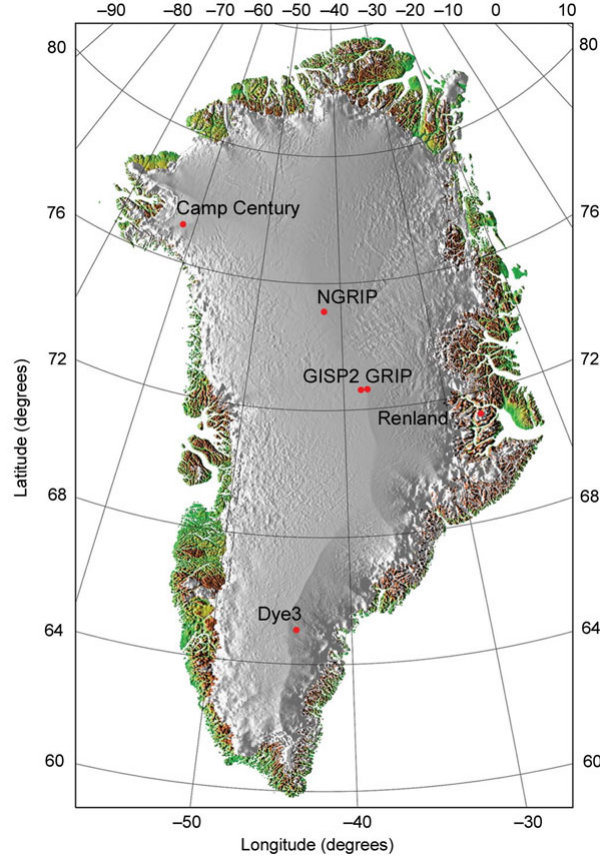
Figure 2.1: Illustration of some of the deep ice core drill sites in Greenland. The site GRIP is in central Greenland (72.5°N, 37.3°W). Figure from [North Greenland Ice Core Project members, 2004].

2.1.2 Total air content estimate

In the introduction the equation showing that the total air content can be calculated from the temperature, pressure and pore volume at close-off is presented (Equation 1.1). The use of this equation is justified since the temperature changes occurring on the surface of the ice sheet (both seasonal and on climatic time scales) are smoothened and can be neglected over the period of the isolation of the pores [Martinerie et al., 1992]. Potentially the temperature and pressure in each individual pore or cluster of pores are different, since the pores become isolated from the atmosphere at different times. If v_k is the air content of a pore under standard pressure and temperature, following relationship for each pore can be written:

$$v_k = v_{ck}\frac{P_{ck}}{T_{ck}} \cdot \frac{T_0}{P_0} \tag{2.1}$$

where v_{ck}, P_{ck} and T_{ck} are the pore volume, the pressure and the temperature of each pore at the isolation from the atmosphere - the close-off. Total air content, V, and pore volume at the close-off, V_c, are defined as:

$$V = \sum_{k=1}^{n} v_k \text{ and } V_c = \sum_{k=1}^{n} v_{ck} \tag{2.2}$$

where n is the number of pores in 1 g of ice. If P_c and T_c denoted mean pressure and temperature at isolation, P_{ck} and T_{ck} can be expressed as:

$$P_{ck} = P_c + \delta P_{ck} \text{ and } T_{ck} = T_c + \delta T_{ck} \tag{2.3}$$

where

$$\sum_{k=1}^{n} \delta P_{ck} = 0 \text{ and } \sum_{k=1}^{n} \delta T_{ck} = 0 \tag{2.4}$$

The total air content can now be written as:

$$V = \frac{T_0}{P_0} \sum_{k=1}^{n} v_{ck} \frac{P_{ck}}{T_{ck}} = \frac{T_0}{P_0} \cdot \frac{P_c}{T_c} \sum_{k=1}^{n} \frac{v_{ck}}{1 + \frac{\delta T_{ck}}{T_c}} + \frac{T_0}{P_0} \cdot \frac{1}{T_c} \sum_{k=1}^{n} \frac{v_{ck} \delta P_{ck}}{1 + \frac{\delta T_{ck}}{T_c}} \tag{2.5}$$

Since the temperature changes, both seasonally and on a climatic time scale, are smoothened strongly, the $\frac{\delta T_c}{T_c}$ term is small (lower than 1%) at close-off and can therefore be ignored. The following is then obtained:

$$V = \frac{T_0}{P_0} \cdot \frac{P_c}{T_c} \sum_{k=1}^{n} v_{ck} + \frac{T_0}{P_0} \cdot \frac{1}{T_c} \sum_{k=1}^{n} v_{ck} \delta P_{ck} \tag{2.6}$$

The second term of this equation can be rewritten by expressing $v_{ck} = \frac{V_c}{n} + \delta v_{ck}$:

$$\frac{T_0}{P_0} \cdot \frac{1}{T_c} \left(\sum_{k=1}^{n} \frac{V_c}{n} \delta P_{ck} + \sum_{k=1}^{n} \delta v_{ck} \delta P_{ck} \right) \tag{2.7}$$

Since $\sum_{k=1}^{n} \delta P_{ck} = 0$ the first term is zero. The second term also becomes zero as it is assumed that the correlation coefficient between the two independent variables δP_{ck} and δv_{ck} is zero. So the whole second term, Equation 2.7, becomes zero and Equation 2.6 only depend on the first term. Equation 2.6 can be written as:

$$V = V_c \frac{P_c \cdot T_0}{T_c \cdot P_0} \tag{2.8}$$

where V_c is the pore volume at close-off ($\frac{\text{cm}^3}{\text{g}}$), P_c is the mean atmospheric pressure at the elevation of the close-off depth, T_c is the temperature prevailing at the close-off, P_0 is the standard pressure (1013 mbar) and T_0 is the standard temperature (273K).

Martinerie et al. (1992;1994) presents data of present day conditions of the pore volume at close-off (V_c) from a large number of sites. Later Delmotte et al. (1999) added some measurements to the data obtained by Martinerie et al. (1992,1994). This plot of pore volume at close-off as a function of temperature from different sites are shown in Figure 2.2. The stars are from Martinerie et al.
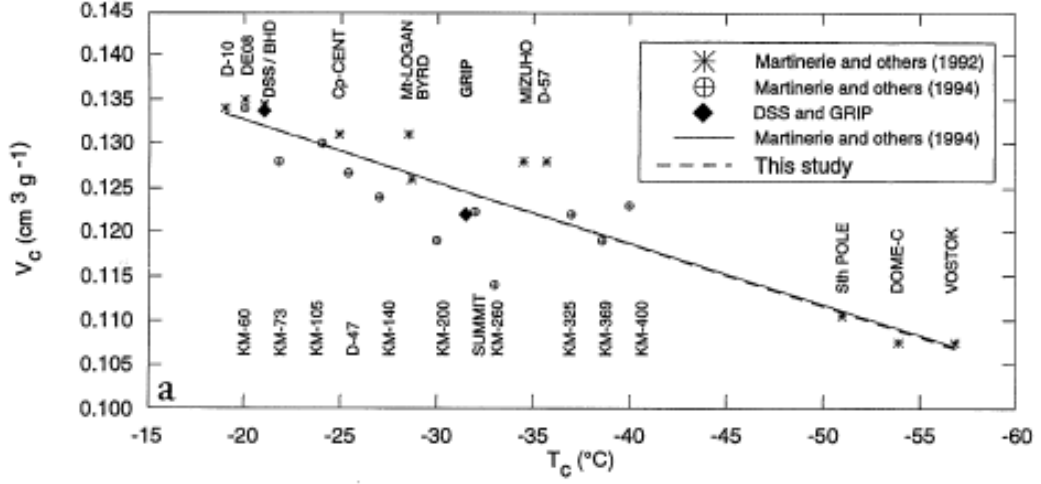
Figure 2.2: Plot of the pore volume at close-off (V_c) versus temperature at close-off (T_c) measured at different drill sites. From [Delmotte et al., 1999].

(1992), the crossed circles are from Martinerie et al. (1994), and the diamonds are added by Delmotte et al. (1999) and are from GRIP and Dome Summit South (DSS). The linear regression obtained from this plot, has the equation:

$$V_c = (6.95 \cdot 10^{-4} \cdot T_c) - 0.043 \tag{2.9}$$

where V_c and T_c are the pore volume and the temperature at close-off respectively. The correlation coefficient of the linear fit is $R = 0.90$ [Delmotte et al., 1999]. From Equations 2.8 and 2.9 and the information from GRIP, and thereby EURO-CORE, (where $T_c = 241.5$ K and $P_c = 660 - 670 mbar$) an expected air content can be calculated. The total air content expected to be measured in the samples from ERUROCORE is $0.0926\frac{cm^3}{g}$.

2.2 Calculating total air content

When experiments are performed the pressure and the temperature of the measuring area are measured. The volume of the system is calibrated beforehand.

From these informations the amount of gas (in this case air n_{air}, with the unit mole) present in the system, after the air has been extracted from the ice, can be calculated from the ideal gas law:

$$P_{meas} \cdot V_{ex} = n_{air} \cdot R \cdot T_{meas} \Rightarrow n_{air} = \frac{P_{meas} \cdot V_{ex}}{R \cdot T_{meas}} \tag{2.10}$$

where P_{meas} is the measured pressure (Pa), V_{ex} is the volume of the measuring area (cm^3), T_{meas} is the temperature of the system (K) and R is the gas constant $(8.3144621 \cdot 10^3 \frac{\text{cm}^3 \cdot \text{kPa}}{\text{K} \cdot \text{mole}})$[1].

Rearranging the ideal gas law equation, the volume of air, V_{air}, can be calculated using standard conditions of temperature ($T_s = 273$K) and pressure ($P_s = 1013$hPa).

$$V_{air} = n_{air} \cdot R \cdot \frac{T_s}{P_s} \tag{2.11}$$

To determine the total air content as a volume of air per mass of ice, $\frac{\text{cm}^3}{\text{g}}$, Equation 2.11 is divided by the mass of the ice, m_{ice}, giving:

$$V_{tac} = \frac{n_{air} \cdot R \cdot T_s}{P_s \cdot m_{ice}} \tag{2.12}$$

where V_{tac} is the total air content of a specific sample with mass m_{ice}. Equation 2.12 will be used to calculate the total air content of the samples, where n_{air} is found from Equation 2.10.

---

[1]The gas constant can be changed according to the units of the other parameters. The units mentioned here are the units that are used in this thesis.

Chapter 3

Experimental setup and procedure

The purpose of the experiment done in this thesis is to measure the total air content of the ice. This is done by extracting the air from the ice in a melt-refreezing process under a vacuum and measuring the change of pressure in a closed off and known volume. When the sample is melted some of the air is dissolved in the water and the sample is then refrozen to push the air out of the water. The air that is now present in the closed system results in an increase of the pressure. The total air content can be calculated from the pressure, temperature and volume.

The experiment in this thesis is a further development of the work by Sebastian Bender (2012), a previous master student at Centre for Ice and Climate.

This chapter describes the experimental setup and procedure. First the previous experimental setup is described, followed by an explanation of the changes that have been made. Then the new setup is described and the experimental procedure is outlined.

3.1 Previous experimental setup

This thesis continues the work of Bender (2012), and the previous experimental setup, built by Bender, can be seen in Figure 3.1. An ice sample is put into an extraction chamber. The extraction chamber is built in the Niels Bohr Institute (NBI) workshop and it is made of aluminium. It has outer dimensions of $42 \times 60 \times 60$mm and inner dimensions of $32 \times 32 \times 32$mm. In Figure 3.2 a picture of the extraction chamber is seen. The corners are rounded, which decreases the inner volume a little, and on the floor inside the chamber there are three (~ 1mm) pikes to prevent ambient air from getting trapped beneath the ice sample when it is placed in the chamber. The extraction chamber is sealed with a black NBR
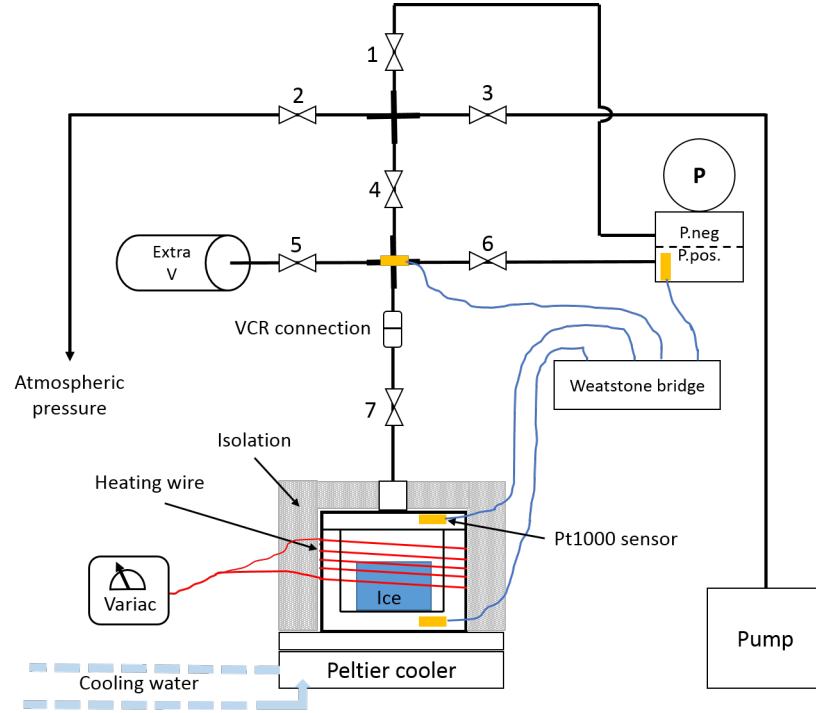
Figure 3.1: Illustration of the experimental setup before any changes has been made. (Drawing based on [Bender, 2012]). A Picture of the setup can be seen in Appendix A.

o-ring[1] from M. Seals that prevents leaks. The lid is then put on the chamber and it is closed with 8 screws. To be able to keep the chamber cold and to freeze the sample the extraction chamber is placed on a Peltier Cooler, that can cool the extraction chamber from the bottom. The Peltier Cooler (build in the NBI workshop) consists of two 3-steps Peltier elements and to obtain a certain temperature difference heat is transferred from one side to another when current is sent through. The warm plate has to be kept cool, since the cooling efficiency depends on the temperature difference, and the warm plate tend to heat up. This is done by pumping cold water through the warm plate with a water pump in a bucket with water [Bender, 2012]. To be able to melt the sample a thin heating wire is wrapped around the extraction chamber. The wire has a resistance of 25Ω. The wire is connected to a variable AC from Advance Instruments, that can apply a known voltage through the wire.

The extraction chamber is surrounded by the isolating material, Armaflex. The chamber can be connected and disconnected to the system by a Swagelok VCR

---

[1]The o-ring has a thickness of 2.4mm, a ring diameter of 41.6mm and a sustainable operating temperature range of $-40°$C to $100°$C.
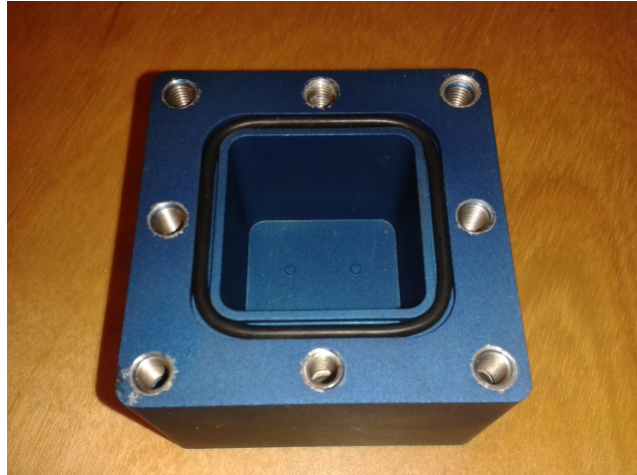
Figure 3.2: Picture of the extraction chamber.

connection. The VCR connection has a Silver-Plated Gasket Retainer Assembly, that has to be changed between every fourth or fifth experiment to avoid leaks.

All tubes are 1/4" stainless steel and seven Swagelok, H-Series (1/4") valves (numbered as seen in Figure 3.1) divide the system into individual sections, that can be closed off. Valve 2 connects the system to the ambient room.

The pressure gauge is a differential pressure gauge of the model Lektra P-BADR, and measures the difference in pressures between the two air inlets, a negative and a positive side. Valves 1 and 6 are both connected to the pressure gauge, respectively the negative and the positive side. The pressure gauge has a resolution of 1 Pa and ranges from -1300Pa to 1200Pa, which means it is a low range pressure gauge. It has a maximum accuracy of 0.075% [Pressure Gauge Manual, 2014].

Valve 5 connects the system to an extra volume. This is necessary because the pressure increase due to the amount of air released from the ice sample sometimes exceeds the range of the pressure gauge. Opening valve 5 will increase the volume of the measuring area which will decrease the pressure. A Duo 2.5 rotary vane pump from Pfeiffer Vacuum is connected to the system via valve 3 to pump air out of the system. The pump can produce a vacuum of 10^{-3}hPa [Operation Instructions; Rotary Vane Pump, 2014].

3.1.1 Temperature measurements

The temperatures of the system are measured with four pt1000 temperature sensors placed on the system. One is placed on the bottom of the extraction chamber and one on the top of it to register the temperatures here and to be able to follow

the difference between those two places. Furthermore a pt1000 temperature sensor is placed on the system just beneath valve 4, and one is placed on the pressure gauge.

The pt1000 temperature sensors are small pieces of platinum connected to 2 wires and the resistance of them is temperature dependent (the resistance of the sensors is 1000Ω at $0°C$). This dependence is close to, but not exactly, linear in the range of temperatures that are relevant in this experiment ($-30°C$ to $30°C$). The Callendar-Van Dusen equation relates the temperature and the resistance in platinum sensors:

$$R = R_0[1 + A \cdot T + B \cdot T^2 + C \cdot T^3 \cdot (T - 100)] \tag{3.1}$$

where T is the temperature ($°C$), R is the resistance (Ω), R_0 is the resistance at $0°C$ (in this case $R_0 = 1000\Omega$), $A = 3.9083 \cdot 10^{-3}°C$, $B = -5.775 \cdot 10^{-7}°C$ and $C = -4.183 \cdot 10^{-4}°C$ when $T < 0°C$ and 0 when $T \geq 0°C$ [Bender, 2012].

Each pt1000 sensor is built into a Wheatstone bridge where the sensor is placed in a circuit with 3 fixed resistors with known resistances. An electromotive force is applied to the circuit, and the voltage across the bridge, that depends on the temperature since the resistance in the pt1000 sensor depends on the temperature, is measured. From this the temperature can be calculated [Bender, 2012].

In a Wheatstone bridge built as shown in Figure 3.3 the voltage across the bridge,
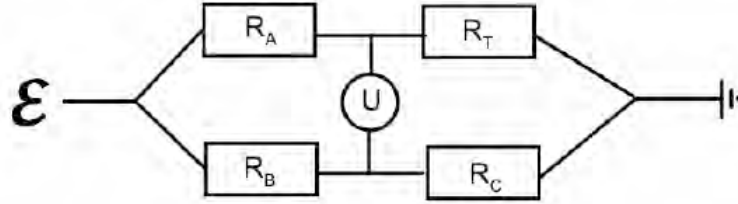
Figure 3.3: Figure of the Wheatstone bridge used to measure the pt1000 sensors resistances. From [Bender, 2012].

U, can be calculated from the electromotive force, and the four resistances in the bridge, R_A, R_B, R_C and R_T as following:

$$U = \varepsilon\left(\frac{R_B}{R_B + R_C} - \frac{R_A}{R_A + R_T}\right) \tag{3.2}$$

The resistances R_A, R_B and R_C are known fixed resistances. The voltage across the bridge, U, and the electromotive force, ε, are being logged. By rewriting Equation 3.2 the temperature dependent resistance in the pt1000 temperature sensors can be calculated from the logged U and ε and the known resistances as:

$$R_T = \frac{\varepsilon}{\left(\frac{\varepsilon \cdot R_B}{R_B + R_C} - U\right)\frac{1}{R_A}} - R_A \tag{3.3}$$

The fixed resistances are determined by Bender (2012), and a Table of these can be found in Appendix B.

3.2 Changes in the setup

A problem with the initial instrumental setup is that not all the air is extracted from the ice in the melting and refreezing process because some of the air is dissolved in the water. In the refreezing process the sample becomes supercooled and suddenly freezes very fast. This results in some of the air being trapped in the ice. If a measurement is done two times in a row (the sample is melted, refrozen and the pressure is measured, twice in a row, pumping the system between measurements) a residual pressure is measured the second time, which would not be the case if all the air had been extracted the first time. To try to compensate for this problem the experimental setup must be expanded. One idea was to change the extraction chamber of aluminium to an extraction chamber where the sides are made of plastic. Here the sample would only freeze from the bottom which would ideally create air free ice. Such a chamber was tested. The chamber consists of three parts: an aluminium bottom, a center part with similar dimensions as the aluminium chamber, but made of plastic, and a lid (same as used for the aluminium chamber). From the tests with this extraction chamber it was found that the leak rate of this box was too high (up to several pascal per minute). This is most likely because the chamber consist of three parts and has to be sealed with o-rings in two places.

Another idea was to trap the air before the pressure gauge so multiple melt-refreeze cycles are possible and the pressure is only measured after more refreezing processes. But the air must still be extracted from the extraction chamber to prevent it from being trapped in the ice again. This idea was pursued.

3.2.1 Trapping the air

To trap the air through several melting and refreezing processes a trap is build. HayeSep porous polymers, that can perform unique separations in gas chromatography (GC) and are usually used for separations of molecules in chemistry, also have the physical property of acting as a gas trapping material. When it is cooled it adsorbs air, and when it is heated the air is released. The characteristics of the physical properties of HayeSep polymers are more reproducible than other competing polymeric products [Vici, HayeSep porouos polymers (2014)]. HayeSep is a powder. In Figure 3.4 a picture of the HayeSep used in this experimental setup is seen. HayeSep is available in many mesh sizes[2] (20-120 mesh). The mesh of

Figure 3.4: Picture of the HayeSep D 20/40 (compared to a ruler (mm lines)).

the HayeSep should be as coarse as possible to decrease the flow rate as little as possible. HayeSep D, 20/40 mesh is used. This corresponds to a mesh between 0.841mm and 0.400mm.

The HayeSep has to be held in place in some way. By placing the HayeSep in a filter the flow area is increased, which increases the flow rate. The mesh of the filter has to fit the mesh of the HayeSep, so the HayeSep is held back by the filter. Since the finer of the HayeSep grains can be 0.400mm the mesh of the filter has to be finer than this to be able to hold back the HayeSep.

The filter used is a 1/4" Inline, F Series Filter with male VCR face seal fittings. Figure 3.5 show the filter and the dimensions of the filter. It is seen in the figure that the air flows in on both the bottom and the sides of the filter. Inline filters are used where space is limited, which is preferable here. The sintered element is replaceable, and both sintered elements ($0.5, 2, 7, 15, 60$ and 90μm) and strained elements ($40, 140, 230$ and 440μm) are available. For this type of filter it is possible to open the filter and fill the sintered/strained element, and in this case the element is filled with HayeSep D 20/40. In Figure 3.5 the filter is a sintered element.

The coarsest sintered element is 90 micron (0.09mm) mesh, but the sintered element can be replaced by a strained element which is available with 230 micron (0.230mm), so a filter with a strained element of 230 micron mesh is used. This was the mesh closest to, but still finer than 0.400mm, available.

An estimate of the inner volume of the filter, where the HayeSep is filled in, is found by measuring the inner dimensions of a sintered element with 90 micron. The diameter is 9.4mm and the depth is 18.9mm. This gives an inner volume of 1311.6mm^3. This approximately corresponds to the amount of HayeSep used. This

---

[2]Mesh size is the number of openings in one inch. As the mesh size increases the particle size decreases; higher mesh size number equals finer powder.
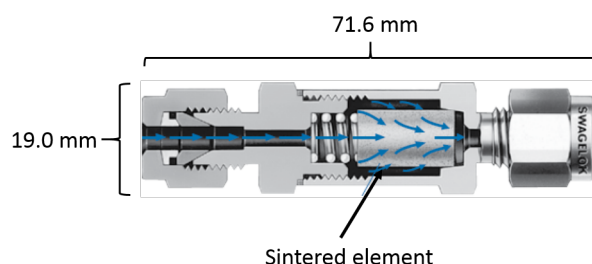
Figure 3.5: The figure shows an Inline, F series filter with a sintered element. The dimensions of the filter are shown and the flow pattern is shown with blue arrows.

is only an estimate since the measurement is done on a sintered element instead of a strained element, but since they both fit in the same filter, the dimensions are expected to be almost alike. The volume of HayeSep used might be a bit larger than the volume of the strained element, since it was filled a bit over the strained element.

In Figure 3.6 an illustration of the filter is seen. The HayeSep was filled in the strained element. To hold the HayeSep in place some quartz wool was put on top of it, and the filter was sealed with a stainless VCR silver plated gasket retainer assembly 60 micron in both ends (this was the coarsest mesh available for that type of gasket). Before the air is trapped the water vapor in the air has to be
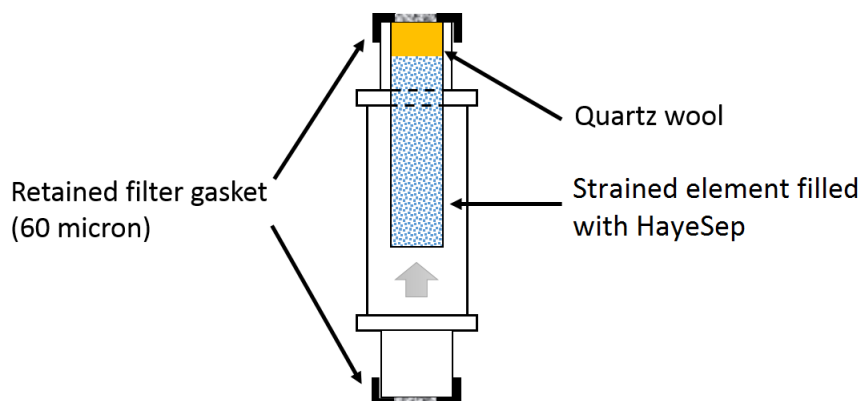
Figure 3.6: Illustration of the air trap. A 230 micron strained element filled with HayeSep D 20/40, held by quartz wool and 60 micron retained filter gaskets.

trapped in order to dry the air. This is done by placing a water trap just before the filter. The water trap was built by putting glass beads in a tube and trapping them with small peaces of stainless steel woven wire cloth. The water trap was

connected to the system with Ultra-Torr vacuum fittings which makes it possible to remove the trap if it needs to be dried. For the water trap to work it has to be cooled to be able to trap the water vapor. This is done by placing a bath with cold ethanol and dry ice[3] in a dewar around the water trap.

To trap the air the HayeSep has to be cooled. This is done by placing a bath of liquid nitrogen (in a dewar) around the filter. Figure 3.7 shows a plot of the pressure decreasing as the HayeSep traps the air. The trapping is slow in the beginning, since the HayeSep is still cooling. Then the process speeds up and after about 2-3 minutes the pressure is very close to zero (still 1-3 Pa). For this last amount of air to get trapped and the pressure to become zero can take 1-3 minutes. To be sure all air is trapped and the pressure has reached complete zero,
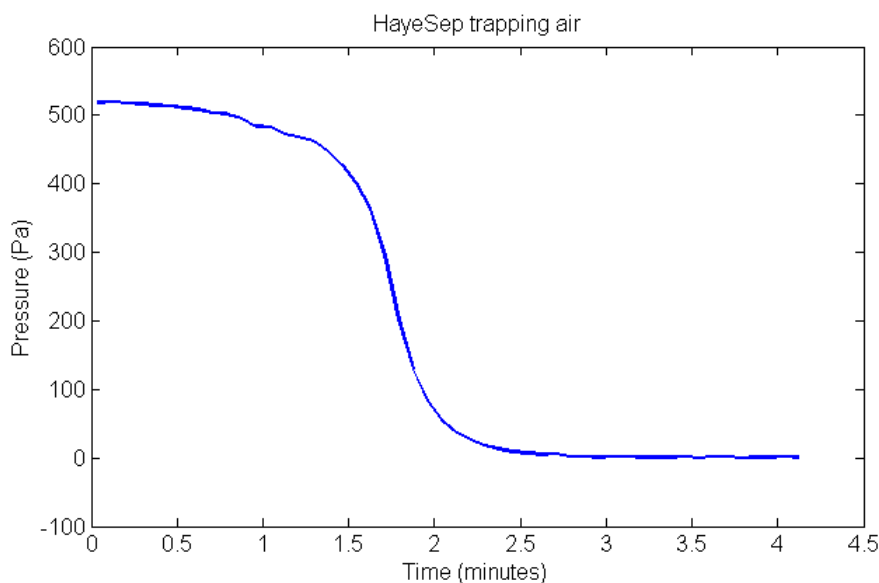
Figure 3.7: The figure shows the air getting trapped in the air trap - filter with HayeSep. The pressure starts at 518Pa and then decreases to almost 0Pa as the HayeSep cools and traps the air.

the liquid nitrogen bath is left around the air trap for 10 minutes.

To quantitatively release the air from the HayeSep it has to be heated. This is done by placing a hot water bath around the area with the filter (see Figure 3.8). Six different tests were made to test the needed water temperature and for how long it should be left around the trap. First a known amount of dry air was trapped in the experimental area (V_{ex} - see Figure 4.5). The air was then trapped in the

---

[3]Ethanol in a dewar is cooled with liquid nitrogen (this makes the cooling process fast) until it is viscous. The dewar is then placed around the water trap and filled with dry ice which keeps the ethanol cooled to around $-78°$C.

HayeSep. A hot water bath was then placed around the filter to release the air. Four temperatures were tested; approximately 50°C, 60°C, 70°C and 80°C. For all four temperatures the water bath was held on for 15 minutes and afterwards the filter was left to reach room temperature to avoid a temperature gradient in the measuring area (V_{ex}). For water baths of 50°C and 80°C the test was done only leaving the bath on for 5 minutes as well. No matter the duration (5-15 minutes) or the temperature of the heating (50-80°C) the pressure reached the initial state when the temperature had equalized. In the experiment a water bath of 50°C to 80°C has to be left around the trap for 10 minutes to be completely sure that all air is released from the trap.

Approximately 1.31cm^3 of HayeSep was used, and since the bulk density of HayeSep D is 0.3311$\frac{g}{cm^3}$ [Vici, HayeSep porouos polymers (2014)], this correspond to 0.44g. The capacity of this amount of HayeSep should be big enough to trap the volume of air in the ice samples, but to be sure a small test was made to find the capacity of the amount of HayeSep in the filter. Dry, ambient air was let into an extra volume connected to the measuring area by valve 10 (se Figure 3.8) so ambient pressure was present in the extra volume ($P_{am} = 1012.1$kPa)[4]. Dry air was produced by activating the water trap with a bath of ethanol and dry ice. Then the measuring area was isolated by closing valve 8. The liquid nitrogen bath was placed around the filter, and valve 10 was opened. To make sure as much air as possible was captured it was left for an hour. The pressure in the measurement area was noted to be 0.251kPa. The air was released with a hot water bath and trapped again two more times to check if the same pressure was reached. The measured pressures were 0.252kPa (second trapping) and 0.249kPa (third trapping). If all the air was trapped the pressure would be zero, but this small pressure indicates that a small amount of air was still present in the system, and not all air was captured.

From this test an estimate of the capacity of the HayeSep could be calculated. The pressure in the extra volume before trapping was known, the pressure after trapping was measured, the temperature in the room was measured ($T_{room} = 293$K), and the volumes of the measuring area ($V_{ex} = 159.39$cm^3) and the extra volume ($V_{cyl} = 120.25$cm^3) were known (these volumes are calibrated in Section 4.2). If n_{all} is the amount of air (in mole) present in the closed system, it can be calculated as:

$$n_{all} = \frac{P_{am} \cdot V_{cyl}}{R \cdot T_{room}} \tag{3.4}$$

where R is the gas constant. The amount of air that was not trapped, the amount

---

[4]This is measured on an absolute pressure gauge, which is described in Section 4.1.2

of free air n_{free}, can be calculated as:

$$n_{free} = \frac{P_{meas}}{R} \cdot \left(\frac{0.9 \cdot V_{ex}}{T_{room}} \cdot \frac{0.1 \cdot V_{ex}}{T_{ln}} \right) \tag{3.5}$$

where P_{meas} is the average of the three measurements, and $T_{ln} = 77°K$ is the temperature of liquid nitrogen. In this calculation the system has to be divided into two parts: the part that was surrounded by liquid nitrogen and therefore had the same temperature as liquid nitrogen, and the rest of the system at room temperature. It was assumed that approximately $\frac{1}{10}$ of the volume was surrounded by liquid nitrogen.

Since the air trapped was the difference between all the air in the system and the free air in the system, the volume of trapped air can then be calculated as:

$$V_{trapped} = n_{all} - n_{free} \cdot \frac{R \cdot T_s}{P_s} \tag{3.6}$$

where T_s and P_s are the standard temperature and pressure. From these equations a capacity volume of the HayeSep used in the experimental setup was calculated to be 111.45cm³. (In this calculation the pressure was corrected according to the pressure gauge calibration equation (Equation 4.3) that is determined in Section 4.1.2).

3.3   The new setup

The new experimental setup is shown in Figure 3.8. The left part of the setup is almost the same as the previous setup. Between valve 6 and the pressure gauge a water trap and then the air trap (filter with HayeSep) were installed. The extra volume, that was previously connected to the system via valve 5, was moved to be connected to the measuring area via valve 10. The extra volume makes it possible to expand the measuring area to increase its volume if the pressure exceeds the range of the pressure gauge. It turned out that this was the case in all the performed experiments. Valve 5, where the extra volume was connected in the previous setup, was sealed with a VCR nut cap.

The extraction chamber previously used was changed to a similar chamber of aluminium because the old extraction chamber had a scratch on top, which resulted in greater leaks. Furthermore the closing procedure of the chamber was changed a bit. The o-ring has to be covered with a thin layer of Dow Corning Corporation low evaporation, High Vacuum Grease[5]. Impurities has to be removed from the top of the extraction chamber and the lid with a brush. The 8 screws sealing the

---

[5]The vacuum grease is a silicone lubricant stable between temperatures $-40°C$ to $204°C$.
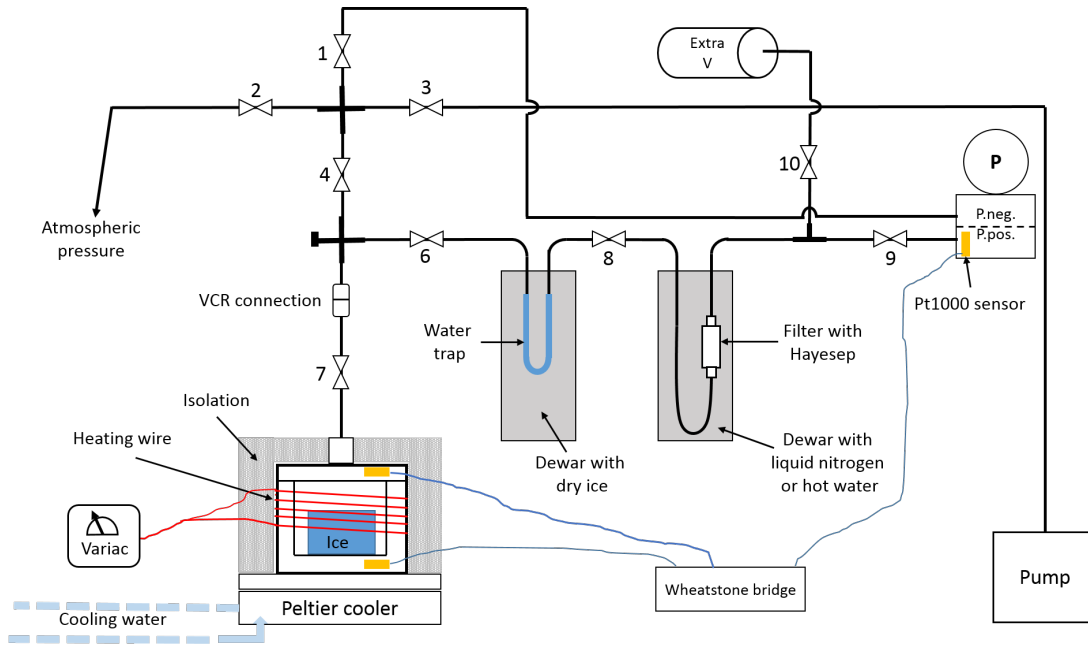
Figure 3.8: Illustration of the new experimental setup. The left part of the system is almost similar to the previous setup but between the extraction chamber and the pressure gauge a water trap and an air trap (filter with HayeSep) is installed. The extra volume is moved so it is connected to the measuring ares (from valve 8 to the pressure gauge). A Picture of the setup can be seen in Appendix A.

lid on the extraction chamber should be closed evenly closing the screws a little at the time, one by one.

The volume from valve 8 to and including the pressure gauge, also including the extra volume, is the measuring area. This means that the extraction chamber is no longer a part of the measuring area as was the case in the previous setup. Therefore the temperatures of the extraction chamber is no longer needed to calculate total air content, only the temperature of the measuring area is needed. However it is still important to know the temperatures of the extraction chamber during the experiment, since this is the only way to know if the sample is melted or frozen.

In Figure 3.9 a plot of the temperature versus experimental time is seen. The blue line is the temperature of pt1000 sensor 1, placed on the bottom of the extraction chamber, and the red line is the temperature of the pt1000 sensor 2 on top of the extraction chamber. The extraction chamber was extracted (pumped free off air) for about 60 minutes after it was connected to the system with a sample inside, while the Peltier cooler was on to prevent the sample from melting during extraction. After being extracted the chamber was isolated by closing valve
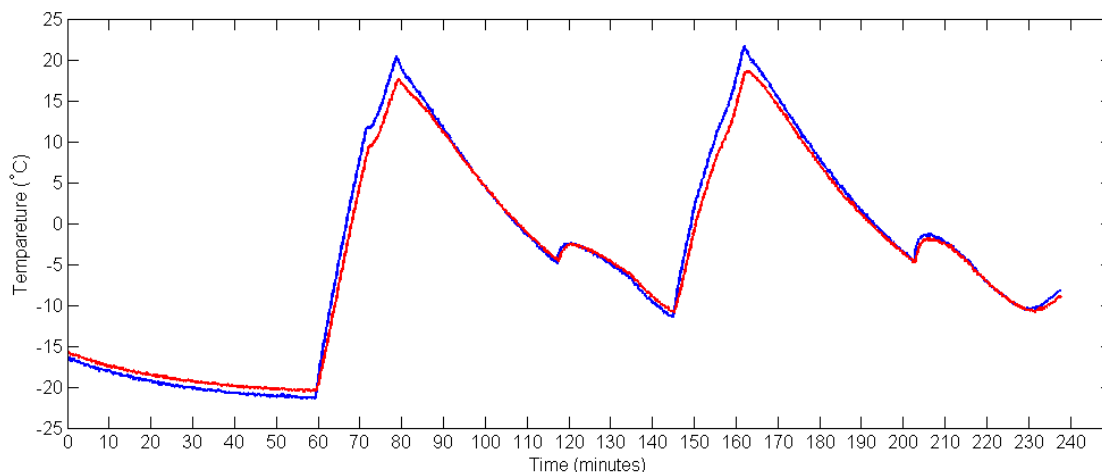
Figure 3.9: Plot of the temperature during the first melting and refreezing cycle of sample 12. The blue line is the temperature of pt1000 sensor 1, placed on the bottom of the extraction chamber, and the red line is the temperature of the pt1000 sensor on top of the extraction chamber. The x-axis show the time duration of the experiment.

7, and the melting process was started. This was done by turning off the Peltier cooler and turning on the heating wire by sending 22 volts through it which gave a heat flux of 20 W. It turned out that if the voltage was turned up to maximum (25 V) the heating wire risked being burned and break, which happened once.

In Figure 3.9 the increasing temperature between 60 and 80 minutes and 145 and 162 minutes is the melting of the sample. The slope of the curve changes after 10-17 minutes, indicating that the sample is completely melted. It is important that the whole sample is completely melted to make sure that all air has escaped from the ice, and therefore the heating wire has to be turned on for 18-20 minutes before it is turned off depending on, when the slope of the curve changes.

In the freezing process the sample freezes from the bottom and the sides. In the process a part of the sample gets supercooled and then suddenly freezes in a very short time. This is seen as a break on the declining curve in Figure 3.9. This break occurs after cooling for 30-40 minutes. In the old experimental setup the extraction chamber had to reach a temperature as low as possible with the Peltier cooler, to decrease the water vapor pressure, and the temperature had to be as stable as possible and should no longer be decreasing, to have a temperature as precise as possible. Since the extraction chamber is no longer a part of the measuring area the stable temperature is not necessary. Furthermore the water vapor pressure (further described in Section 3.4) should no longer be a problem since a water trap is installed between the extraction chamber and the air trap.

In the new setup it is only necessary that the whole sample is completely frozen before the trapping of the air from the sample is started. Therefore the extraction chamber is kept closed for 45-60 minutes for the sample to be completely frozen, depending on when the break on the curve occurs. Before valve 7 is opened and the extraction chamber is in connection with the measuring area and the air trap, the liquid nitrogen bath can be put around the trap for the HayeSep to be around $-196°$C and working as a trap. This will speed up the trapping process.

Generally the melting of the sample is a bit faster in the second cycle (this is also seen in Figure 3.9). This is partly because the extraction chamber and the sample inside is not as cold when the second melting cycle is started as it is when the first melting cycle starts. However, it is also because the sample is more closely in contact with the inner walls of the extraction chamber in the second cycle. The three small nubs on the floor of the extraction chamber keeps the sample lifted a small bit above the floor, and the sample either has no contact with the side walls or is only in contact on one of the sides. In the following cycles (2., 3., etc.) the sample has been fluent and is therefore in contact with both the floor and the walls. This also means that the temperature, at which the sample is completely melted, is a bit lower than it is in the first cycle.

When the air has been released from the air trap by placing a hot water bath around the filter, a temperature gradient occurs in the measuring area. To get rid of this gradient and obtain a constant temperature in the whole measuring area, this part of the system is left for 40-60 minutes to reach room temperature. The process can be sped up by placing a dewar with water at room temperature around the filter for 5-10 minutes. This can be done while the sample is being remelted and refrozen since these two parts of the system are not connected during the melting/refreezing cycle.

The pt1000 temperature sensors have been shown to have internal heating [Bender, 2012]. Therefore the temperature measurement has to be stopped for a couple of minutes before the final temperature measurement is done simultaneously, with the pressure being noted manually. The temperature is then the instantaneously logged temperature.

3.3.1 Outline of experimental procedure

The day before an experiment is done the o-ring is taken off the extraction chamber and the bottom side of the lid and the top of the extraction chamber are cleaned, and the extraction chamber and the lid are cooled by putting them in the freezer (the o-ring is not put in the freezer, since it is less flexible when it is cold). A VCR cap is put on the VCR connection instead of the extraction chamber and the system is set up to be evacuated during the night (all valves, except for valve 2, are opened).

On the day of the experiment the following procedure is followed:

1. The Peltier cooler and the water pump is turned on. This is done to precool the Peltier cooler so it is already below freezing point when the extraction chamber is placed on top of it. A cold ethanol bath with dry ice is placed around the water trap.

2. Valve 4 and 6 are closed (to avoid getting ambient pressure into the system), and the VCR cap is taken off.

3. In the freezer the dimensions of the ice sample are measured and the sample is put in the chamber.

4. The o-ring is covered with a thin layer of vacuum grease and placed on the extraction chamber.

5. The lid is put on and the screws are tightened as evenly as possible.

6. Valve 7 (the valve connected to the extraction chamber) is closed and the extraction chamber is placed in an isolation box and brought to the lab, fast, but carefully.

7. The extraction chamber is connected to the system, valve 1 is closed and valves 4 and 7 are opened for the extraction chamber to be evacuated. Valve 6 is opened so the pressure in the extraction chamber is known and to make sure all the air is extracted from the system (the pressure gauge should reach its zero). The system is left to evacuate for 60 minutes.

8. After 60 minutes valve 7 is closed to isolate the extraction chamber from the rest of the system.

9. The Peltier cooler is turned off and the heating wire is turned on by sending 22 volts through it. It is turned on for 20 minutes.

10. After 20 minutes the heating wire is turned off and the Peltier cooler is turned on again to cool for 45-60 minutes (depending on when the break on the curve occurs - when the sample is completely frozen).
    While the ice freezes a dewar with liquid nitrogen is put around the air trap.

11. After 45-60 minutes valve 4 is closed and valves 6, 7 and 8 are opened. The air is now being trapped in the HayeSep. It is left like this for at least 10 minutes. The valves 6, 7 and 8 are then closed again.

    The melting and refreezing process can now be repeated while the air is released from the trap.

12. The Peltier cooler is turned off and the heating wire is turned on for 20 minutes.

13. While the sample is melting the air is released from the trap: the liquid nitrogen bath is removed and a dewar with hot water (60°C to 80°C) is put around the air trap and left for 10 minutes.

14. After 10 minutes the hot water bath is now removed and the filter is left to reach room temperature as the rest of the system (this process can be sped up by placing a dewar with room temperature around the filter for 5-10 minutes).

15. When the temperature has equalized, the pressure is registered and the temperature is measured by the pt1000 sensor on the pressure gauge.

16. Items 10, 11, 13, 14 and 15 are performed again, respectively. Step 12 is only performed if more than 2 melting/refreezing cycles are done.

The sample can now be melted and refrozen as many times as needed. To test how many melting/refreezing cycles are necessary to extract all air, 3 samples were melted and refrozen 4 times. The pressure is measured between every melting/refreezing cycle to see the change in pressure. In all 3 tests a pressure change of 1-3 Pa (randomly) was seen after the third and the fourth cycle, which correspond to a raise in pressure of less than 0.5% of the pressures of about 500Pa measured in the experiments. Since the pressure change is so low and it is the same for the third and fourth cycle, it is assumed to be due to leaks.
Throughout the experiment it is important to check the temperature of the water in the bucket with the water pump, sending water through the Peltier cooler, regularly, since the water is heated up by the Peltier cooler. If the water becomes warm the Peltier cooler can be overheated, so the water has to be changed during experiments.

3.4 Vapor pressure

The vapor pressure is the pressure at which a gas can coexist with its condensed phase (liquid or solid) in a closed system. The vapor pressure is exponentially dependent on the temperature. In Table 3.1 some values of the vapor pressure of ice at different temperatures are shown.

When the extraction chamber is evacuated the system is opened to the pressure gauge (valve 6, 8 and 9 are open), so the pressure can be detected during the evacuation and to make sure the system and the chamber are completely evacuated before the first melting and refreezing process is started. As a result of the vapor

Temperature (°C)	Pressure (Pa)
-20	103.24
-22	85.08
-24	69.89
-26	57.24
-28	46.72
-30	38.01
-32	30.81
-34	24.89
-36	20.04
-38	16.07
-40	12.84
-60	1.081
-70	0.262
-75	0.122
-80	0.055

Table 3.1: Table showing the vapor pressure of ice at different temperatures. The table only shows values in the appropriate ranges [Haynes, W.M., 2014].

pressure a pressure is detected on the pressure gauge. This will be a pressure between 20 and 50 Pa depending on the temperature in the extraction chamber.

During the experiment all water vapor is trapped in the water trap that is cooled by a bath of ethanol cooled with dry ice which has the temperature of approximately $-78°$C. The water trap now contains the surface area that emits a vapor pressure over ice which is $-78°$C here. According Table 3.1 the vapor pressure at $-78°$C is between 0.122 and 0.055 Pa, and since the resolution of the pressure gauge is 1 Pa, the vapor pressure will not be detectable. This is tested by putting the cold ethanol bath around the water trap before the extraction chamber, with a sample inside, is connected to the system. The pressure detected at the pressure gauge, when the extraction chamber and the whole system are completely evacuated, should then correspond to the zero of the pressure gauge.

In the previous experimental setup the water trap was not a part of the setup, and the pressure was measured above the ice sample. In that case the vapor pressure had to be taken into consideration, since the vapor pressure at the measuring temperature (around $-25°$C to $-30°$C) is 70Pa to 38Pa. The vapor pressure in the new setup should not be detectable and can therefore be neglected.

However it seems there is a problem with the water trap. When the extraction chamber is evacuated with a sample inside, the pressure does not reach the zero

point of the pressure gauge, but stabilizes at a point 5-10 Pa above the zero point. This indicates that the water trap is not completely efficient. To test if the efficiency is related to the temperature of the ethanol bath it was replaced with a liquid nitrogen bath. The pressure decreased 2 Pa, but this decrease in pressure could be a result of temperature change in the water trap area, and the pressure was still not reached zero. Using a bath of liquid nitrogen might result in gases of the air being trapped, so it was decided to keep using the cold ethanol bath since it did not seem to change the error much. Because the offset from zero changes between experiments it is not possible to correct for this error.

3.5   Leaks

It is almost impossible to produce a completely leak tight system. After building the new parts of the system leaks were detected in all the new parts. A few connections were changed, and all connections where tightened. Afterwards the leaks in these parts were very low.

   The leak rate in the system was tested by evacuating the whole system, closing all valves and leaving the system for 25 hours. The measuring area (closed valve 8 and open valve 9 and 10) turned out to be close to leak tight; during 25 hours the pressure did not change. In the whole system a leak of 16 Pa was detected. Most of this leak came from the extraction chamber. This leak corresponds to a leak rate of 0.6 Pa per hour.

   It was acknowledged that the closing procedure of the box was important to minimize leaks in the extraction chamber. The chamber, the lid and the o-ring had to be cleaned to remove vacuum grease from the previous experiment, and then dusted off with a brush to make sure potential dust and small hairs were removed. The o-ring has to be covered with a thin layer of vacuum grease, the lid put on and the screws closed evenly, a little at a time.

   Some of the experiments were performed with more than two melting and refreezing cycles. The residual pressures measured after these extra cycles were almost similar and it is therefore expected to be leaks. Therefore a leak rate was calculated from these residual pressures. In Table 3.2 the extra cycles and their time duration and residual pressures are shown. From this, leak rates for every cycle are calculated and finally the average leak rate is calculated. The average leak rate is $1.584\frac{\text{Pa}}{\text{h}}$, which is higher than the leak rate measured in the 25 hours test. This might be because the temperatures of the extraction is varied (about $-30°$C to about $30°$C). This might affect the o-ring and result in higher leaks than when the box is left at a constant temperature (room temperature, which is not expected to vary more than a few degrees during 25 hours). Since the temperature changes occur during experiments, this is the leak rate used to correct the measured

Experiment	Cycle nr.	Time duration (h)	Pressure (Pa)	Leak rate (Pa/h)
1	3.	1.50	3	2.000
	4.	1.50	2	1.333
2	3.	2.75	2	0.727
3	3.	1.33	2	1.504
	4.	1.33	2	1.504
4	3.	1.33	1	0.752
	4.	1.50	1	0.666
5	3.	1.33	3	2.256
	4.	1.33	4	3.008
	5.	1.33	2	1.503
	6.	1.33	3	2.256
	7.	1.33	2	1.503
Average:				$1.584\ \frac{Pa}{h}$

Table 3.2: Table showing the leaks from experiments with more than 2 cycles.

pressure in the results.

Chapter 4

Calibrations

To calculate the total air content the pressure and the volume of the system are needed. The pressure of the system is measured with a Lektra P-BADR differential pressure gauge. Bender (2012) showed that 1 Pa on the pressure gauge was close to but not exactly one pascal. It was therefore necessary to calibrate the pressure gauge which is described in the first part of this chapter. In the second part the calibration of the volumes of the system is described.

4.1 Calibrating the pressure gauge

4.1.1 Problems with the pressure gauge

During the period of this thesis a problem with the pressure gauge occurred a couple of times. This made the calibration indispensable. The problem was that the pressure difference was not always zero when the two sides where openly connected, which is to be expected since it is a differential pressure gauge, meaning that it measures a pressure difference between to inlets. When the pressure gauge had atmospheric pressure on both the negative and the positive sides, (V_{neg} and V_{pos}), the pressure gauge showed a differential pressure close to the zero of the gauge, -0.009 to-0.005kPa. But when the whole system was evacuated and the negative and positive side is openly connected, the gauge showed a pressure below zero (eg. -0.300kPa). When a small amount of air is let into the system the pressure gets closer to zero, but not all the way. This indicates that the shift seemed to be pressure dependent.

The problem occurred several times, and it seemed to emerge when a big inequality in the pressures on the negative and the positive sides was present over a longer period (a couple of days): for example when the negative side was evacuated and the positive side was left at atmospheric pressure. It is possible that

the problem is due to some kind of shift in the sensing diaphragm, that bends proportional to the applied pressure, but this has not been verified.

These problems makes it important to redo the calibration of the pressure gauge, and it might even be necessary to calibrate it every time this problem has emerged. Fortunately the problem did not occur after the pressure was calibrated.

After having problems with the pressure gauge the zero point of the pressure gauge had shifted from being 0 to being around -0.009 to -0.005kPa. This is seen when the negative and the positive sides are openly connected, and the pressure stabilizes at a small negative pressure. Before every experiment the whole system is evacuated completely, and the small negative shift, the new zero point denoted P_{diff}, is noted and then subtracted from the measured pressure.

4.1.2   Calibration procedure

To calibrate the pressure gauge an absolute pressure gauge is needed. A Digiquartz Portable Pressure Standard of the model $760-23A$ from Paroscientific Inc. is used. It consist of a Digiquartz Pressure Transducer that provides high accuracy pressure measurements; full scale accuracy of 0.001% or better. The Portable Standard has a range of $0-23$ psia[1], and a resolution of 0.0001% [Digiquartz Portable Standard Manual, 2014]. This absolute pressure gauge is referred to as 'Portable Standard', while the Lektra pressure gauge connected to the system will continuously be refeered as 'the pressure gauge'.

A system is set up connecting the pressure gauge and the Portable Standard with a volume that can change size in between. Here a plastic bottle, that can be squeezed, is used. A drawing of the setup is shown in Figure 4.1. In the experimental setup the system is usually connected to the ambient room via valve 2. The line connected to valve 2 is now extended with a 1/8" stainless steal tube, that is connected to the Digiquartz Portable Pressure Standard with a VCO Swagelok connection. The line is also connected to a flexible plastic bottle (see Figure 4.1). This connection is done with a SMC 6×4 polyurethane air tube. The bottle is connected to the ambient room with a polyurethane air tube that can be closed off with a tube cap. The connections on the bottle and between the plastic tube and the steal tube are very leaky, so a valve is put in to be able to seal the system with the two pressure gauges (see Figure 4.1). When the bottle is squeezed the system changes volume and the pressures on the two pressure gauges should change equally.

Ambient air was let into the whole system by taking the tube cap of the tube on the bottle and opening the external valve (valves 1, 2, 4, 6, 8 and 9 were open, valves 3, 7 and 10 were closed). The ambient pressure, P_a, was measured on the

---

[1]psia is pounds per square inch absolute and this correspond to a range of $0-15.858$kPa
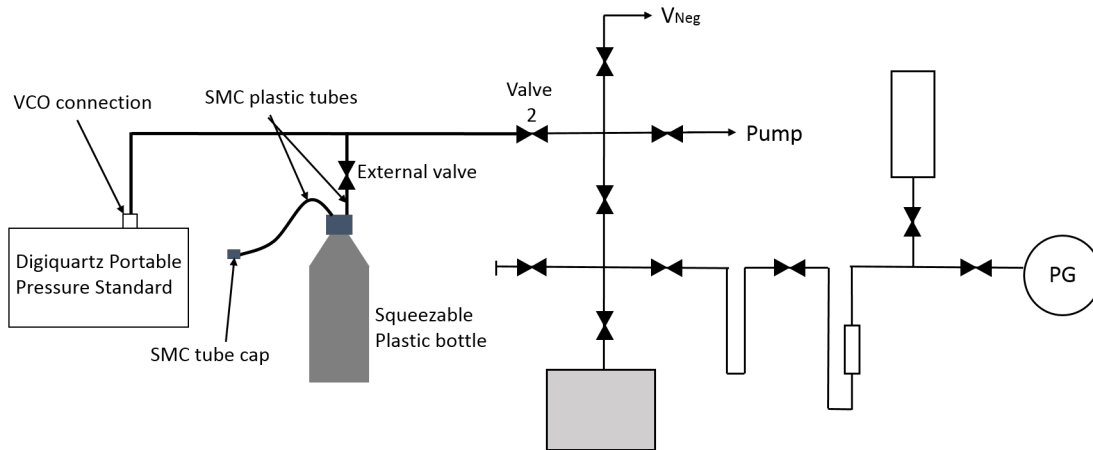
Figure 4.1: Drawing of the setup used to calibrate the pressure gauge. The two pressure gauges are connected with a squeezable bottle in between.

Portable Standard. Valve 1 was closed slowly and ambient air was now present in V_{neg}.

The tube cap was put on the bottle to enclose the system, and the bottle was then squeezed together. This decreased the volume of the system, and the pressure rose out of the range of the pressure gauge. The external valve was closed and the tube cap was taken off the bottle. Now air was slowly let into the system by opening the external valve. When the pressure reached the range of the pressure gauge, the external valve was closed, and when the pressures of the pressure gauge and Portable Standard had stabilized, they were noted. Repeatedly, small amounts of air was let in by opening and closing the external valve and noting the pressure when they had stabilized until ambient pressure occured in the system.

For the negative range of the pressure gauge to be calibrated, the pressure had to go beneath zero, which was done by closing the external valve, squeeze the bottle and put the tube cap at the end of the tube. The external valve was then opened and the pressure went down to the minimum range (-1300Pa). Air was now let in a little at the time by opening the external valve. When the pressure moved into the range of the pressure gauge, the external valve was closed and the pressures of the pressure gauge and Portable Standard were noted. The external valve was opened again to let in a bit of air to increase the pressure and the pressures were noted again. This was repeated until ambient pressure was reached.

To be able to determine a one-to-one relation between the registered pressures from the two pressure gauges, the ambient pressure that was let into V_{neg}, P_a is subtracted from the Portable Standard pressure. This is now the pressure difference between the ambient pressure at the beginning of the experiment and the measured pressure on the Portable Standard. This difference is plotted against the

measured pressure on the pressure gauge (P_{diff} is subtracted from this pressure before it is plotted). The plot is seen in Figure 4.2 The black dots show the data,
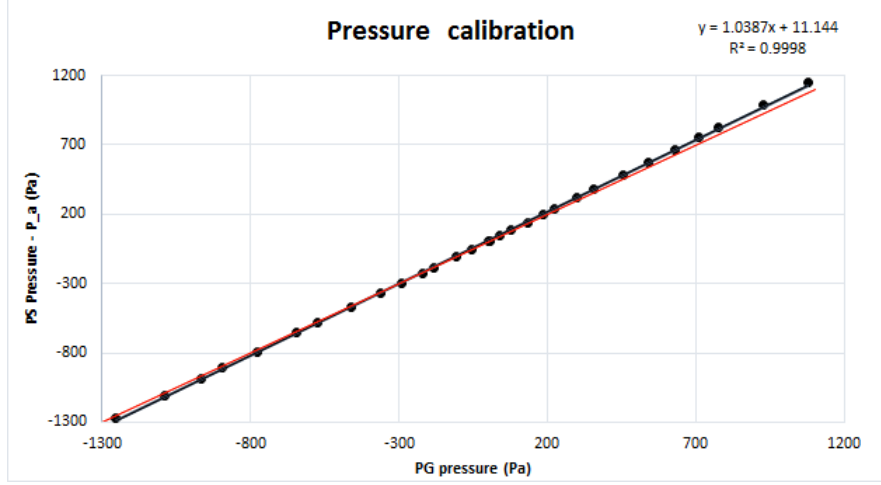
Figure 4.2: Plot of the pressures from the calibration. The pressure difference between the Portable Standard pressure and the ambient pressure, P_a, plotted against the pressure of the pressure gauge. The black dots show the data, the black line is a linear fit of the data line, and the red line represents a one-to-one relation showing where the data data should be if 1 Pa on the pressure gauge was exactly equal to 1 Pa on the Portable Standard. The linear regression is shown in the upper right corner.

and the black line is a linear fit of the data line. The coefficient of determination of the linear fit is $R^2 = 0.9998$. The red line represents a one-to-one relation showing where the data should be if 1 Pa on the pressure gauge was exactly equal to 1 Pa on the Portable Standard. It is clear from the plot that this is not the case, but it is not far from a one-to-one relation. This means that the measured pressures have to be corrected for this offset in the pressure gauge. This is done by calculating a calibrated pressure from the regression equation in Figure 4.1:

$$P_{cal} = 1.0387 \cdot P_{meas} + 11.144 \tag{4.1}$$

where P_{meas} is the measured pressure, and P_{cal} is the calibrated pressure. The standard error of this fitting can be calculated by:

$$\sigma_y = \sqrt{\frac{1}{N-2} \sum_{k=1}^{n} (y_i - B - A \cdot x_i)^2} \tag{4.2}$$

where N is the number of measurements, x_1 and y_i are the measured points $(x_1, y_1), ..., (x_N, y_N)$, A is the slope of the fitted line, and B is the intercept with the

y-axis [Taylor, 1997]. For this fit we get a standard error for the calibrated pressure of 8.59, indicating that the uncertainty is $\pm 8.59 Pa$. Including the subtraction of P_{diff} in the regression equation, which is done prior to the linear regression in Equation 4.1, we get:

$$P_{cal} = 1.0387 \cdot (P_{meas} - P_{diff}) + 11.144 \tag{4.3}$$

The pressures are logged via a National Instrument Logger as voltages. To be able to calculate the pressure from the logged voltage a small calibration was done. Dry air was let into the measuring area. This air was produced by activating the water trap with a ethanol and dry ice bath. The system was then pumped until the pressure reached the range of the pressure gauge, and valve 8 was closed. When the pressure had stabilized it was noted manually. Valve 8 was opened just a little to pump air out of the system and then closed again, and the pressure was noted when the pressure had stabilized. This was repeated until the pressure reached zero. The logged voltages are shown in Figure 4.3 The averaged voltages
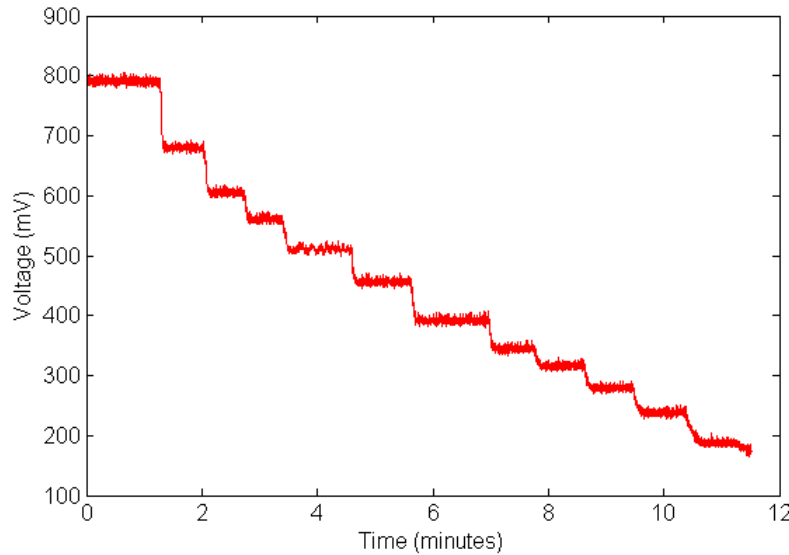
Figure 4.3: A plot of the voltage against time (minutes) as the air is pumped from the system a little at the time.

from the different levels are plotted against the manually noted pressures. This plot is seen in 4.4. The black dots represent the data points, and the black line is the linear regression line fitted to the data. The linear regression equation is used to calculate the pressure from the logged voltages.

$$P_{log} = 1926.7 \cdot v_{log} - 307.14 \tag{4.4}$$

where P_{log} is the logged pressure and v_{log} is the logged voltages.
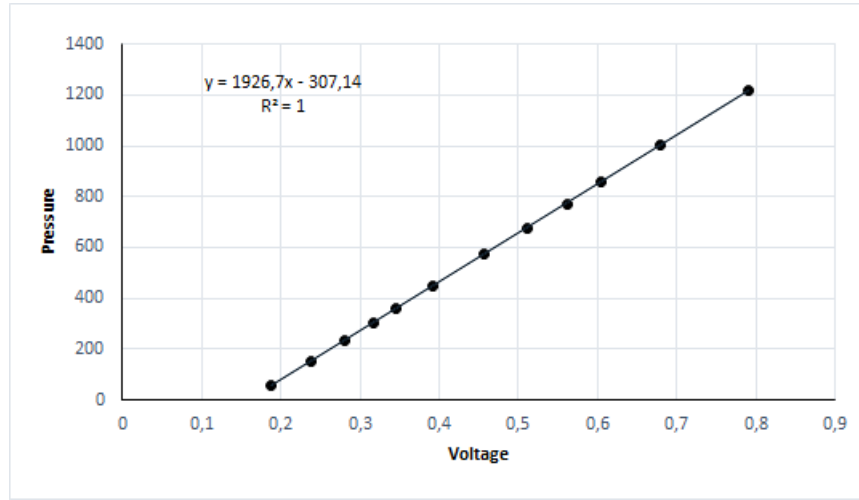
Figure 4.4: A plot of the logged voltages against the manually noted pressures. The black dots are the data points, and the black line is a linear regression.

4.2   Calibration of volumes

To be able to calculate the total air content the volume of the measuring area in the experimental setup has to be known. An estimate of the measuring area is 152.5cm^3. This is found by multiplying the inner volume of the tubes $(0.22\frac{\text{cm}^3}{\text{cm}})$ with the length of tube in the measuring area ($\sim 110\text{cm}$). The inner volume of the filter is estimated to be 10cm^3, and the volume of the extra volume is by Bender (2012) calibrated to be 118.28cm^3. These three volumes added give an estimated volume of 152.5cm^3. To determine a more exact volume of the measuring area was calibrated. This was done by performing a row of measurements where the volume in the whole system is changed a bit by having different sizes of small steal balls inside the extraction chamber. Three different steel balls are used. Their dimensions are seen in Table 4.1.

Ambient dry air was let into the measuring area. The pressure exceeded the

Ball	Diameter (cm)	Volume (cm^3)
B_{15}	1.5	1.7671
B_{20}	2.0	4.1888
B_{25}	2.5	8.1812

Table 4.1: Table showing the diameter and volume of the three steel balls used for the volume calibration.

range of the pressure gauge so the system was pumped until the pressure was in the range, and valve 8 was closed so the pressure could stabilize. The pressure (P_1) was noted, and valve 10 was then closed to isolate the extra volume with the known pressure. The rest of the system was then completely evacuated till the pressure gauge reached its zero point. Valve 8 was then closed, and valve 10 could be opened expanding the air only present in the extra volume, V_{cyl}, to the measuring area, V_{ex}. When the pressure had stabilized, this pressure (P_2) was noted. Valve 8 was then opened expanding the air to the whole system, V_t, with valves 1, 2, 3 and 5 closed and all other valves opened. When the pressure had stabilized, this pressure (P_3) was noted (in Figure 4.5 the different volumes of the system is seen). This procedure was performed with various combinations of the
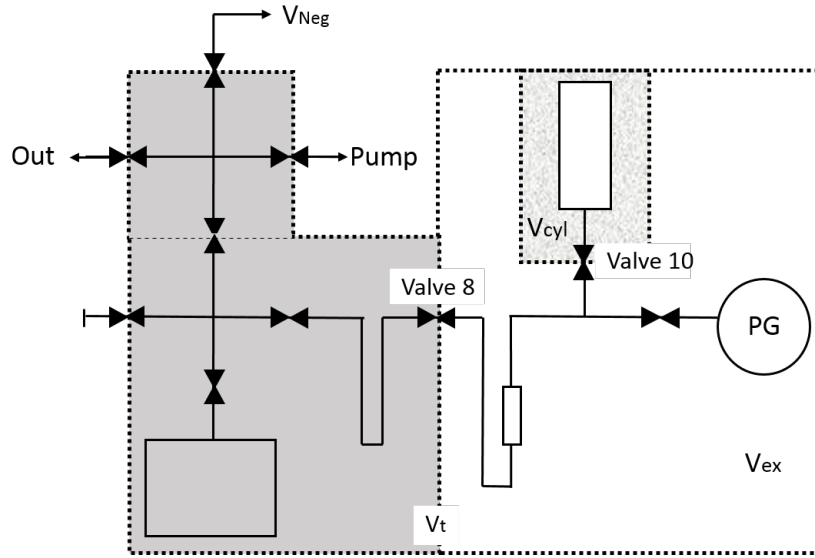
Figure 4.5: The experimental setup divided into volume areas. V_{cyl} is the extra volume, V_{ex} is the measuring area that includes V_{cyl}, and V_t os the total volume of the system.

steel balls in the extraction chamber changing the volume of V_t. Since $B_{15} + B_{20}$ and $B_{15} + B_{25}$ fit in the chamber together, six different volumes of V_t were possible:

- $V_t - 0 \rightarrow$ no balls in the extractions chamber.

- $V_t - B_{15} \rightarrow B_{15}$ in the extractions chamber.

- $V_t - B_{20} \rightarrow B_{20}$ in the extractions chamber.

- $V_t - B_{25} \rightarrow B_{25}$ in the extractions chamber.

- $V_t - B_{15+20} \rightarrow B_{15}$ and B_{20} in the extractions chamber.

- $V_t - B_{15+25} \to B_{15}$ and B_{25} in the extractions chamber.

Since the same amount of air occurs in the system, the following is valid:

$$P_1 \cdot V_{cyl} = P_2 \cdot V_{ex} = P_3 \cdot V_t - B \tag{4.5}$$

where B denotes the total volume of balls inside the extraction chamber. To calibrate the volume of the measuring area the following is obtained:

$$P_2 \cdot V_{ex} = P_3 \cdot (V_t - B) \Rightarrow V_{ex} = \frac{P_3}{P_2} \cdot V_t - \frac{P_3}{P_2} \cdot B \Rightarrow V_{ex}\frac{P_2}{P_3} + B = V_t \tag{4.6}$$

This can be rearranged to:

$$B = V_t - V_{ex}\frac{P_2}{P_3} \tag{4.7}$$

which is an linear equation where V_{ex} is the slope of the line, and V_t is the intercept, where B and $\frac{P_2}{P_3}$ are obtained from a row of calibration experiments. Figure 4.6 is a plot of B against $\frac{P_2}{P_3}$ where the dots are the data, and the line is the leaner regression. The regression equation gives a volume of $V_{ex} = 159.39\text{cm}^3$ and
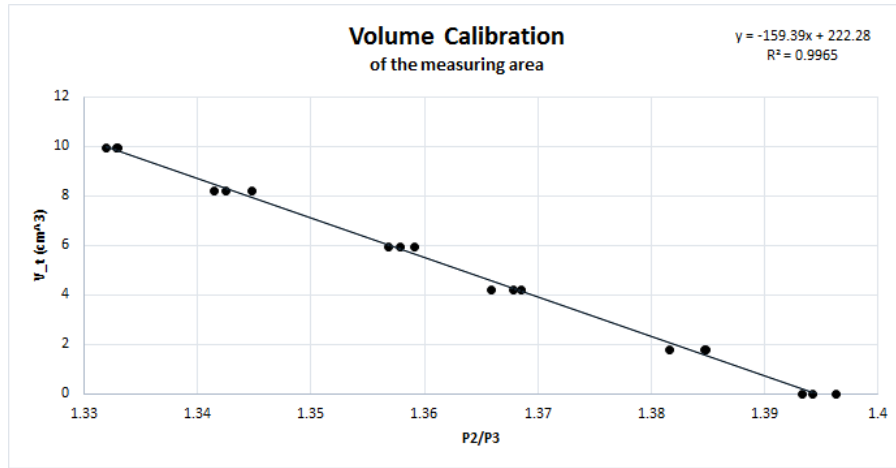
Figure 4.6: Plot of B against $\frac{P_2}{P_3}$ where the dots are the data and the line is the leaner regression. The regression equation is seen in the upper right corner.

$V_t = 222.28\text{cm}^3$. The coefficient of determination is $R_2 = 0.9965$. The standard error of the slope of the linear regression is 2.36 giving an uncertainty of V_{ex} of $\pm 2.36\text{cm}^3$. The standard error of the intercept of the linear regression is 3.22 giving an uncertainty of V_t of $\pm 3.22\text{cm}^3$.
In the same way the volume of V_{cyl} can be obtained:

$$B = V_t - V_{cyl}\frac{P_1}{P_3} \tag{4.8}$$

In Figure 4.7 a plot of B against $\frac{P_1}{P_3}$ is seen and from linear regression $V_{cyl} = 120.25\text{cm}^3$. The total volume is obtained again from this regression giving $V_t = 221.96\text{cm}^3$. The coefficient of determination is $R_2 = 0.9949$. The standard error of

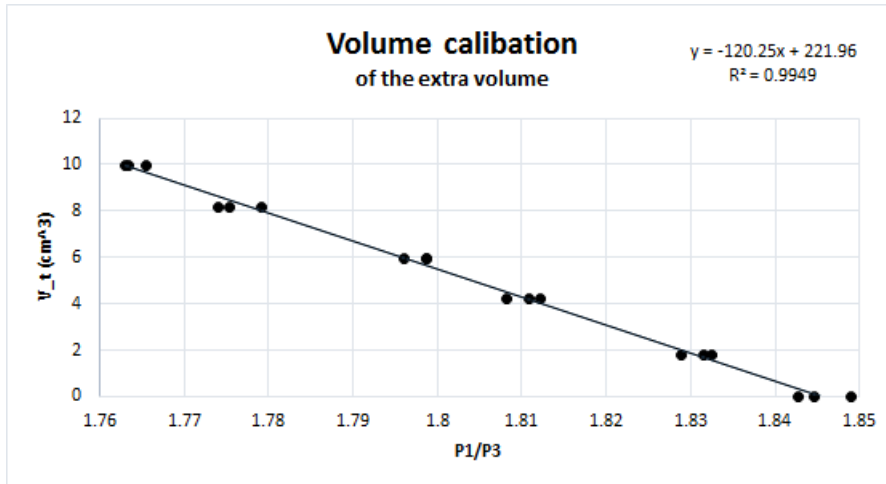**Figure 4.7:** Plot of B against $\frac{P_1}{P_3}$ where the dots are the data and the line is the leaner regression. The regression equation is seen in the upper right corner.

the slope of the linear regression is 2.15 giving an uncertainty of V_{cyl} of $\pm2.15\text{cm}^3$. The standard error of the intercept of the linear regression is 3.89 giving an uncertainty of V_t of $\pm3.89\text{cm}^3$.

Chapter 5

Ice samples and cut bubble effect

In this chapter information about the samples that are measured in this thesis is presented. Afterwards the problem of the cut bubble effect is described and determined for the measured samples.

5.1 Sample dimensions and masses

The samples, that are measured, are cut from a piece of ice core from EUROCORE from approximately 280 m below surface (mbs). The samples were cut as big as possible from the core piece. This resulted in samples with side length of approximately $24 \times 24 \times 18$mm. A few of the samples vary 1 mm in side lengths. Since the extraction chamber has inner dimensions of $32 \times 32 \times 32$ mm the samples fit into the chamber. In the cutting process some smaller pieces were cut off not to be used because they had cracks, which could influence the total air content.

Prior to the experiments the samples have been weighed on a weight measuring the mass in gram with 2 digits, so the error is estimated to be 0.01g. In Table 5.1 the sample numbers and their respective depth, dimensions and weight are shown.

From the same piece of core samples were cut and $\delta^{18}O$ was measured for comparison with the results. The $\delta^{18}O$ record from the piece of core is shown in Figure 5.1. It seems that the core piece contains approximately two summer layers (the optima of the curve) and three winter layers (the minima of the curve) corresponding to $2\frac{1}{2}$ years.

Sample nr.	Depth (mbs)	Dimensions (cm)	Weight (g)
4	280.045	$2.4 \times 2.4 \times 1.8$	9.69
5	280.095	$2.4 \times 2.4 \times 1.8$	9.43
6	280.120	$2.4 \times 2.4 \times 1.8$	9.43
8	280.180	$2.4 \times 2.3 \times 1.8$	9.69
9	280.205	$2.4 \times 2.4 \times 1.9$	9.66
10	280.230	$2.4 \times 2.3 \times 1.9$	9.60
11	280.255	$2.4 \times 2.3 \times 1.8$	9.29
12	280.305	$2.4 \times 2.4 \times 1.8$	9.63
13	280.330	$2.4 \times 2.3 \times 1.8$	9.39
14	280.355	$2.4 \times 2.4 \times 1.8$	9.40
15	280.380	$2.4 \times 2.3 \times 1.8$	9.26

Table 5.1: Table showing information about the samples
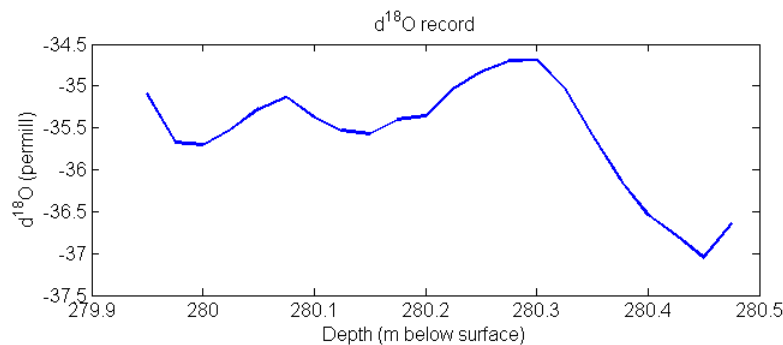
Figure 5.1: $\delta^{18}O$ record against depth from the same piece of core the total air content samples are from.

5.2   Cut bubble effect

When the samples are cut some of the bubbles are cut open. The air from these bubbles are then lost. This results in a significant bias when measuring the total air content. In this experiment it results in lower air content measurements due to the air that is lost. Down through the ice sheet the bubble sizes decrease due to the increasing pressure from the layers of ice above. Therefore the cut bubble effect decrease rapidly with depth. Deeper in the core the gas molecules become entrapped as gas hydrates [Martinerie et al., 1990], but since EUROCORE is a shallow core and the bubbles obviously are present in the ice (see Figure 5.2) this is not relevant for this study. The cut bubble effect from same depth but at different sites can differ due to the bubble sizes varying at different sites. For

example colder sites generally have a larger number of small bubbles than warmer sites [Martinerie et al., 1990].

Total air content measurements can be corrected for the cut bubble effect if the size of the samples and the size and the shapes of the bubbles are known.

The ratio between the number of cut bubbles on a unit surface area, n_c, and the total number of bubbles per unit volume, n_t, can be linked to the mean size of a convex bubble (meaning the distance between two parallel planes oriented at random, and tangential to the bubble), $< H >$, by a calculation based on a statistical relation [Martinerie et al., 1990]:

$$\frac{n_c}{n_t} =< H > \tag{5.1}$$

From Equation 5.1 the following can be derived if the sample is cubic and has side lengths A:

$$\frac{N_c}{N_t} = \frac{6 < H >}{A} \tag{5.2}$$

where the surface area is $6A^2$. N_c is the number of cut bubbles in the cube and N_t is the total number of bubbles in the cube (including cut bubbles).

Since the bubbles on average are assumed to be cut in the middle the air that is lost from a cut bubble correspond to half the volume included in N_c, meaning $\frac{N_c}{2}$. A percentage of the gas that is lost can be obtained from:

$$\frac{V - V_{meas}}{V} = \frac{N_c}{2 \cdot N_t} \tag{5.3}$$

where V_{meas} is the measured air content and V is the total air content corrected for cut bubbles. This can be written as:

$$\frac{V - V_{meas}}{V} = \frac{1}{2} \frac{n_c}{n_t} \frac{s}{v} \tag{5.4}$$

(s being the surface area and v being the volume of the sample) which can be used for samples of any form [Martinerie et al., 1990]. To be able to calculate the percentage of gas lost the total number of bubbles and the number of cut bubbles in a sample has to be known. It turned out to be impossible to count the number of cut bubble on the surface of the sample. On the surface of the sample small grooves appeared which made it difficult to see bubbles on the surface that were cut. Some cut bubbles were visible but it was not possible to determine if the visible cut bubbles were all the cut bubbles in this area or just some of the bubbles. Some thin slices (2-3 mm) of ice from the core were cut and pictures were taken of these and one of these pictures is seen in Figure 5.2. On the close-up pictures it was not possible to see which bubbles were cut and which were not.
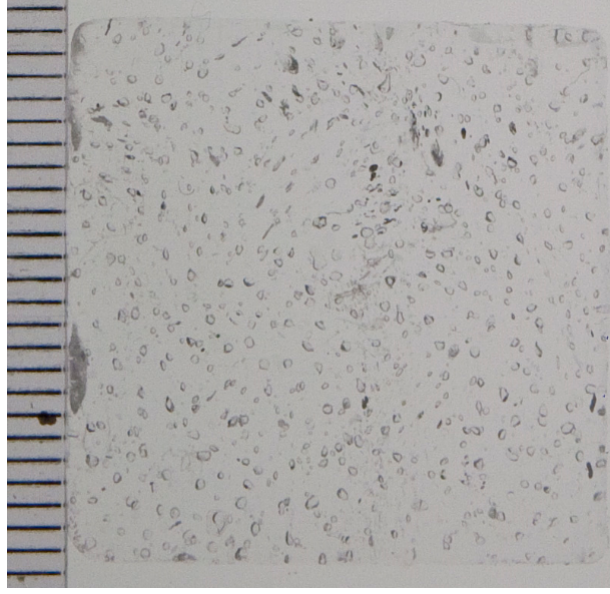
Figure 5.2: Picture of a thin slice of ice from. The piece is $2.4 \times 2.4 \times 0.3$cm. The bubbles in the ice are seen clearly. The lines on the left are mm lines from a ruler.

Assuming that the bubbles are all spherical the mean diameter, $< D >$, of the bubbles will be equal to $< H >$ and from Equation 5.2 and 5.3 the percentage of gas lost can be found as:

$$\frac{V - V_{meas}}{V} = \frac{3 < D >}{A} \tag{5.5}$$

Using the calculated mean diameter value and the side length of the samples the percentage of gas lost can be obtained by using Equation 5.5.

In Figure 5.2 it is seen that the bubbles have different sizes and shapes. Most of the bubbles though have a shape that is close to spherical. To simplify it is therefore assumes that the bubbles are spherical. To be able to calculate the percentage of gas lost by using Equation 5.5, the mean diameter, $< D >$, of the bubbles in the samples has to be determined.

The bubble size decrease with depth but in the relatively short depth range of the samples measured in this thesis (0.34 m) it is assumes that the size of the bubbles and the cut bubble is the same for all the samples. From the close-up pictures of the thin ice slices it was possible to determine $< D >$ by measuring the diameter of the bubbles in a small area and find the mean value. In a small area of 5×5mm a number of 30 bubbles are measured to have a mean diameter of 0.39mm. The samples have side lengths of $24 \times 24 \times 18$mm meaning that they are not cubic. Using Equation 5.5 to calculate the cut bubble effect assuming a side

length of 24mm the cut bubble effect will be 4.88%. But since the samples are not cubic this will underestimate the cut bubble effect. By determining a relationship between the surface area and the volume of cube and of the samples a multiplying factor can be found for Equation 5.5. For relatively large samples compared to the bubble size it can be assumed that the number of cut bubbles n_c is proportional to the surface area v:

$$n_c = \alpha \cdot v \tag{5.6}$$

where α is a constant. The total number of bubbles in the sample, n, is proportional to the volume v:

$$n = \beta \cdot v \tag{5.7}$$

where β is a constant. For a cubic sample the relation the between n_c and n can be determined as:

$$f_{cut_{cube}} = \frac{n_c}{n} = \frac{\alpha}{\beta} \cdot \frac{s_{cube}}{v_{cube}} = \gamma \frac{s_{cube}}{v_{cube}} \tag{5.8}$$

where s_{cube} in the surface of a cube and v_{cube} is the volume of a cube. The same applies for a non cubic samples:

$$f_{cut_{sample}} = \gamma \frac{s_{sample}}{v_{sample}} \tag{5.9}$$

where γ is a constant independent on the sample shape. The relationship between these fractions for a cubic and the samples determine the difference between the cut bubble effect of a cubic sample and a non cubic sample:

$$\frac{f_{cut_{sample}}}{f_{cut_{cube}}} = \frac{s_{sample}}{v_{sample}} \frac{v_{cube}}{s_{cube}} \tag{5.10}$$

For a cubic sample the surface area is $s_{cube} = 6 \cdot A^2$, where A is the side length, and volume is $v_{cube} = A^3$ and the surface area can be expressed by the volume of the sample as:

$$s_{cube} = 6 \cdot v^{\frac{2}{3}} \tag{5.11}$$

If it is assumes that the volume of the cubic sample corresponding to a sample of this thesis must be the same, $v_{cube} = v_{sample}$, the following is valid:

$$\frac{s_{sample}}{s_{cube}} = \frac{s_{sample}}{6 \cdot (v_{sample})^{\frac{2}{3}}} \tag{5.12}$$

For a sample with side lengths $2.4 \times 2.4 \times 1.8 \times$ this relation becomes 1.0095. The side length of a cubic sample with the same volume as the samples can be determined by from $v_{cube} = A^3 \Rightarrow A = \sqrt[3]{v_{sample}}$ giving a side length of $A = 2.18$. Using this A in Equation 5.5 and multiplying by the fraction determined by Equation 5.12 the cut bubble effect is determined to be 5.42%.

Studies show that the cut bubble effect is usually between 10% at the close-off and 1% several hundred meters beneath the surface [Martinerie et al., 1990]. This is in agreement with the calculated cut bubble effect of 5.42%.

Chapter 6

Results

In this chapter the results from the experiments will be presented. Before the total air content is calculated the measured pressure has to be corrected for the shift in the pressure gauge, and leaks and the calculated air content should be corrected for cut bubble effect.

6.1 Experimental results

To calculate the total air content the following steps of calculations are conducted. The amount of air present in the measuring area is calculated from Equation 2.10. The volume of the measuring area is calibrated to be $V_{ex} = 159.39\text{cm}^3$. The temperature is calculated by converting the logged voltages across the Wheatstone bridge to a resistance via Equation 3.3. The temperature is then calculated from the resistance via the Callendar-Van Dusen Equation 3.1. The measured pressures has to be corrected. First the pressure is corrected for the small offset from zero on the pressure gauge. This offset is noted before every experiment. Then the pressure is calibrated by the pressure calibration equation found in Section 4.1.2. Equation 4.3 corrects the measured pressure both for the offset from zero and the calibration.

The calibrated pressure is then corrected for the leaks that occur in the extraction chamber. This is done by subtracting the leak rate $1.584\frac{\text{Pa}}{\text{h}}$ (calculated in Section 3.5) multiplied by the experimental time, from the calibrated pressure. The experimental time, where leaks in the extraction chamber occur, is the time from the chamber is isolated after extraction, to the time where the measuring area is isolated from the chamber with the extracted air trapped in the air trap.

From this calibrated and leak rate corrected pressure, the amount of air, that is present in the measuring area after it has been extracted from the ice sample, can be measured using Equation 2.10. Equation 2.11 then converts the amount of

air into a volume by using standard values of pressure and temperature and divide it with the mass of the sample to get a total air content per g of ice in the sample.

The total air content is finally corrected for the cut bubble effect by adding 5.3% to the total air content. These calculated total air contents of the samples are shown in Table 6.1. In Figure 6.1 a plot of the total air content calculated between

Sample nr.	Depth	Total air content
	mbs	$\frac{\text{cm}^3}{\text{g}}$ of ice
4	280.045	0.0922
5	280.095	0.0905
6	280.120	0.0915
8	280.180	0.0860
9	280.205	0.0838
10	280.230	0.0877
11	280.255	0.0885
12	280.305	0.0897
13	280.330	0.0896
14	280.355	0.0835
15	280.380	0.0855
Average		0.0881 $\frac{\text{cm}^3}{\text{g}}$ of ice

Table 6.1: Table of the calculated air content and the corresponding depth of each sample.

the different corrections is seen. The red line represents the total air content calculated from the raw pressures that are manually noted in the experiments. The green line is the total air content calculated from a pressures corrected for the offset from zero at the pressure gauge and the pressure calibration. The black line is the total air content calculated from a pressures corrected for the offset, the pressure calibration and leaks. The blue line is the final result of the total air content corrected for cut bubble effect.

Figure 6.2 show the final result (blue line and dots) with all corrections against a plot of the $\delta^{18}O$ record (green line) from same depths.
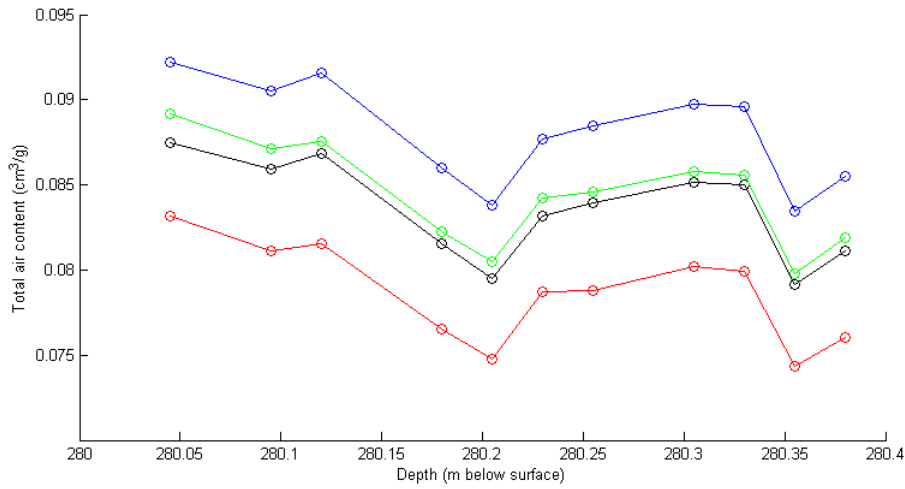
**Figure 6.1:** A plot of the total air content calculated between the different corrections. The red line and dots are the total air content calculated from the raw pressures that are manually noted. The green line and dots are total air content calculated from a pressures corrected for the offset from zero at the pressure gauge and the pressure calibration. The black line and dots are the total air content calculated from a pressures corrected for the offset, the pressures calibration and leaks. The blue line and dots are the final result of the total air content corrected for cut bubble effect. All are plotted against depth (m below surface).
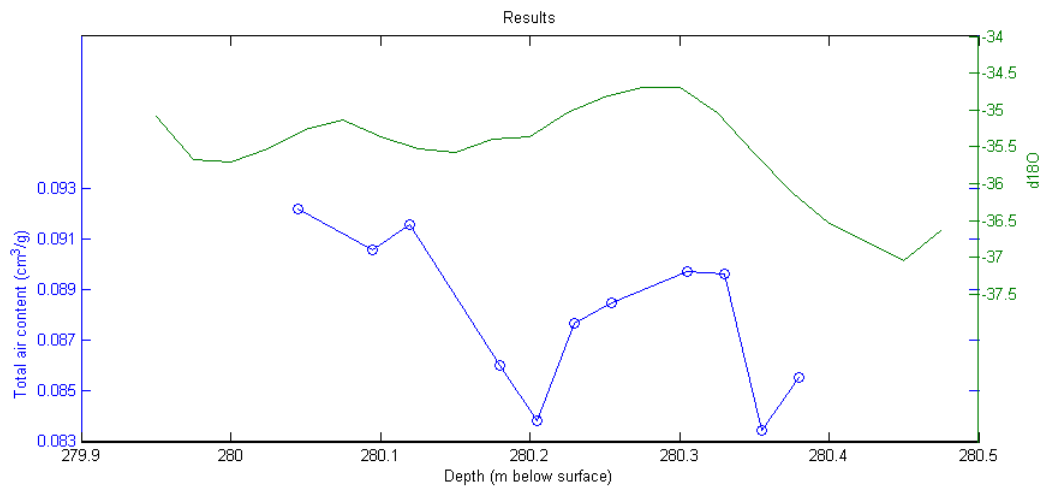
Figure 6.2: A plot of the final results, where the blue dots represent each sample and the blue line connects these dots, and $\delta^{18}O$ record (green line) from the same depths.

Chapter 7

Discussion

In this chapter the experiment and the results are discussed. First the advantages, disadvantages and the errors of the new experimental setup are discussed. Then the correction of the cut bubble effect is discussed. The results obtained in this thesis are discussed and compared to results from other studies. Finally improvements to the experimental setup are suggested.

7.1   Expansion of the experimental setup

The experimental setup by Bender (2012) has been improved by an extension with a water trap and an air trap. The air trap is built up by putting HayeSep polymers in a filter and works as expected: When the air trap is cooled with a bath of liquid nitrogen it traps the air, and when it is heated with a bath of hot water, $50-80°C$, all the air is released again. The capacity of the HayeSep is found to be $111.45cm^3$ which exceeds the volume of air extracted from the samples greatly since this is less than $1cm^3$.

The air trap now has the function of trapping the air in between melting/re-freezing cycles. The extension of the experimental setup has some other essential advantages. In the new experimental setup the extraction chamber is no longer a part of the measuring area. This has two major advantages. First of all, the volume of the measuring area no longer changes according to the ice sample. Though the ice samples have almost the same dimensions, their volumes are not exactly the same. This would change the volume of the measuring area in the previous setup since the samples where a part of the measuring area, that thereby changed volume according to the volume of the sample. Also a small part of the samples might evaporate during the extraction of the extraction chamber, changing the volume of the sample during an experiment. This is no longer the case in the new setup. Secondly, it means that the temperature in the experimental area no longer

range from the temperature of the extraction chamber (-30 to $-25°C$) to room temperature. In the previous setup the temperature in the extraction chamber was held cold by the Peltier cooler, and the rest of the system was at room temperature. This meant that a temperature gradient was present in the system. In the previous experimental setup it was assumed that the extraction chamber had the temperature measured on the chamber, and the rest of the system, the tubes, were at room temperature. This neglects the temperature gradient that will occur in an open system with different temperatures. In the new experimental setup the extraction chamber and the cold temperature present there is no longer a part of the measuring area. In the new setup a temperature gradient still occurs in the measuring area when the air trap is cooled or heated to trap or release the air. But before the measurements are made the measuring area is left for 30-45 minutes to reach room temperature, and a temperature gradient in this part of the system no longer present. This advantage also simplifies the calculations of the total air content.

The extraction chamber no longer being a part of the measuring area also means that the temperature of the extraction chamber does not have to reach a state of stable temperature, which was the case in the previous setup. In the new setup it is only necessary to make sure that the sample is completely refrozen. This takes 30-40 minutes and it is clearly seen as a break on the temperature curve. This is an advantage since it shortens the duration of an experiment. The duration of the experiment is 4 to 5 hours. In this time two cycles of melting and refreezing are performed. This is almost half the time of the previous experimental setup. There the refreezing process alone could take around two hours because the temperature had to be as low as possible to decrease the water vapor pressure and the temperature had to stabilize for the temperature measurement to be stable. Still the experimental time is long for a measurement of one sample. It is thus difficult to perform more than one experiment per day. Besides only one extraction chamber with a lid is available, so two experiments in one day can not be done, since the box have to be emptied, dried and cleaned and then cooled down to be ready for a new experiment. With one more identical extraction chamber available it might be possible to perform measurements of two samples in one day.

The new built in air trap makes it possible to do several melting/refreezing cycles and trapping the extracted air in between the cycles. When the sample refreezes, the air present in the extraction chamber, is the air that has been extracted in the prior melting process. From experiments with three, four and seven melting/refreezing cycles it was clarified that the majority of the air is released in the first cycle. The observed pressure change in the third cycle and upwards is approximately similar and is therefore concluded to be due to leaks in the extraction chamber. The observed pressure change between the first and the second

cycle is high enough (5 to 10Pa) to conclude that it is air that has been retrapped in the ice during the first refreezing. This probably happens because some of the air is dissolved in the water. During the second refreezing cycle very little air is present in the extraction chamber, since this is only the air from the second melting process. Therefore the amount of air that can be dissolved in the water during the freezing is very small, and since the observed pressure changes in the following cycles are assumed to be due to leaks, the solubility is completely neglected.

The leak rate that is calculated from the pressure changes from the third cycle and upwards is found to be $1.584\frac{Pa}{h}$. This is higher than the leak rate found from the 25 hours experiment, where the system was left to leak and a leak rate of $0.6\frac{Pa}{h}$ was found. This increase in the leak rate during experiments is most likely because the temperatures vary from $-30°C$ to $25°C$ which stresses the o-ring and can create leaks between the extraction chamber and the lid.

When the samples are refrozen the water freezes from the bottom and sides, and the last water in the middle is supercooled and freezes suddenly, which produces a break on the temperature curve (seen in Figure 3.9). This sudden freezing creates cracks in the ice. In Figure 7.1(a) a picture of the sample after several melting/refreezing cycles is seen. The middle part of the sample has many small cracks and some bigger cracks spreading from the middle, which verifies this sudden freezing. Figure 7.1(b) show another sample where the sudden refreezing process has resulted in a kind of small explosion producing a pike of ice sticking up in the air.

(a) 1   (b) 2
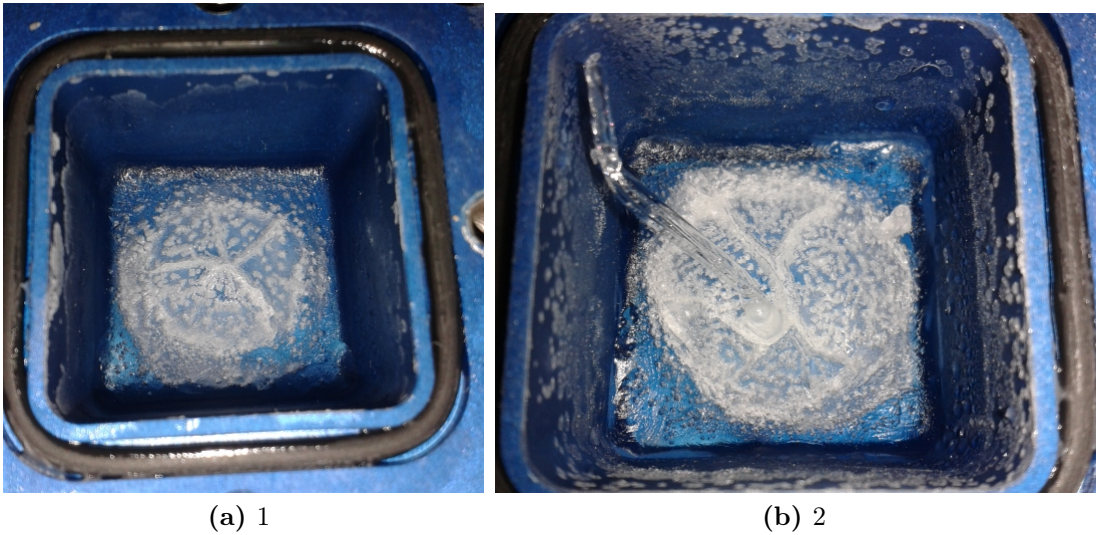
Figure 7.1: Picture of the sample in the extraction chamber after an experiment, where the sample is 'exploded' in the freezing process and produce an ice pike.

A water trap was built into the system before the air trap to dry the air before it is trapped. This should decrease the water vapor pressure to be below 1 Pa, since the surface omitting water vapor pressure is now at $-78°$C (the temperature of the ethanol bath with dry ice), in stead of it being the sample in the extraction with temperatures of -30 to $-25°$C omitting a water vapor pressure. However, it turned out that the water trap was not working optimally. When the system was set up to evacuate with a sample in the extraction chamber, and valves open to be able to register the pressure in the system, the pressure did not reach zero as it was expected. Instead a pressure of 5-10 Pa above the zero point of the pressure gauge was registered. This is lower than the water vapor pressure of a sample of -30 to $-25°$C ($38 - 69$Pa), indicating that the water trap is working, but not working optimally. The pressure is not corrected for this error since it did not seem to be constant, but changing between experiments. It might have been possible to correct for it if this pressure due to vapor pressure was registered just before valve 7 was closed and the melting/refreezing process was started. Unfortunately this was not done and beside it might have been changing during experiments.

Once it was tested, if the registered water vapor pressure was due to the temperatures of the trap not being cold enough, by placing a bath of liquid nitrogen around the trap having the temperature $-196°$C (the temperature of liquid nitrogen) instead of the $-78°$C of the ethanol bath. The pressure decreased 1-2 Pa, but this decrease was probably due to the big decrease in temperature of the trap. To avoid the possibility of trapping other parts of the air than the water vapor, and because it did not seem to make a difference, it was decided to keep using the ethanol bath.

7.1.1   Uncertainties

The pressure gauge measures the pressure with an accuracy of 0.075%. This is lower than 1 Pa for all pressures within the range of the pressure gauge ($-1300 - 1200$Pa). Since the precision of the pressure gauge is 1 Pa, the accuracy is lower than the precision. For the calibration of the pressure gauge done in comparison with an absolute pressure gauge the linear regression has a coefficient of determination $R^2 = 0.9998$. This is very close to 1 indicating that the linear fit is good. The calibrated pressures from the measured pressures in the experiments lie between $514 - 593$ Pa with a mean value of 550 Pa. The calibrated pressure has an uncertainty of ± 8.59 Pa determined from the linear regression. This gives a resultant error of the pressure of 1.56%.

The volumes of the system were also calibrated. The volume of the measuring area, V_{ex}, the extra volume, V_{cyl}, and the total volume of the system, V_t, are all determined from the same row of measurements. First the volume of the measuring area was calibrated to be $V_{ex} = 159.39$cm^3 with an uncertainty of ± 2.36cm^3.

From the linear fit determining V_{ex} the total volume of the system was found to be $V_t = 222.28\text{cm}^3$ with an uncertainty of $\pm 3.22\text{cm}^3$. Afterwards the volume of the extra volume was determined to be $V_{cyl} = 120.25\text{cm}^3$ with an uncertainty of $\pm 2.15\text{cm}^3$. From this linear fit the total volume was also found. Here the total volume was calibrated to be $V_t = 221.96\text{cm}^3$ with an uncertainty of $\pm 3.89\text{cm}^3$. There is a small difference between the two calibrated volumes of V_t (0.32cm^3). This difference lies within the uncertainty determined for both volumes, and the difference is small indicating that the calibrated volumes are good.

The total volume of the system is not used in any of the calculations. The volume of the extra volume is used to calculate the capacity of the HayeSep. The extra volume was also calibrated by Bender (2012) to have a volume of 118.28cm^3. Since the cylinder was only moved, the volume of this should not change. But there is a small difference of 1.97cm^3 between the the two calibrations. This small difference lies within the small uncertainty of V_{cyl} $(\pm 2.15\text{cm}^3)$. This indicates that both calibrations are good. The volume of the measuring area V_{ex} is the most important volume. The uncertainty of $\pm 2.36\text{cm}^3$ compared to the volume of 159.39cm^3 gives an resultant error of 1.44%.

A change in temperature will change the volume of the measuring area since the steal of the tubes will expand or contract. But since the measuring area is at room temperature, when the measurements are taken, the temperatures will not change more than a couple of degrees, and the resultant volume change is assumed to be so small that it can be neglected.

The masses of the samples are measured on a weight measuring with two digits. The uncertainty of the mass is estimated to be ± 0.01g since the weight would sometimes jump between two digits during measurements. Compared to the samples with masses between $9.26 - 9.69$g and a mean value of 9.50g this results in a error of 0.11%.

The temperature sensors were calibrated by Bender (2012), but it turned out, that due to internal heating in the temperatures during the whole calibration, the calibration equations were invalid. This was realized too late to be able to recalibrate the temperature sensors. The calibration equations determined by Bender (2012) can be found in Appendix C. Since the internal heating in the pt1000 temperature sensors was not accounted for in the calibration, temperature calculated with the calibration equations will be too high.

During the period of making experiments a thermocouple connected to a PID controller (proportional-integral-derivative controller) registered the room temperature just beside the measuring area. These temperatures were noted, when the final measurement was taken and range between $20-21°$C. Calculating the temperatures from the logged voltages using the calibration equations the temperatures lie between $24-25°$C. This is approximately $4°$C higher than the logged temper-

atures confirming that the calibration equations seems to calculate temperatures that are too high.

To calculate the total air content the temperatures are calculated from the voltages using the standard Callendar-Van Dusen equation (Equation 3.1 in Section 3.1.1). This is not completely correct since the constants are not found for these pt1000 sensors. The temperatures calculated using the standard equation lie between $21 - 22°$C. This is only one degree different from the temperatures measured with the PID. It is therefore concluded that using this equation to calculate the temperatures from the logged voltages do not give temperatures that are completely wrong in the range of room temperature. Besides a change in the temperaure of 1°C will only change the total air content results 0.3%. The uncertainty of the temperature is estimated to be ±1°C giving a resultant error of 0.34% compared to the room temperature of 294K.

To determine an overall error of the experiment from the individual errors a general equation, finding the error ΔY of the function $Y = f(x_1, x_2, ..., x_n)$ from the individual errors Δx_i of the values x_i, is used [Lipenkov et al. 1995]. The equation looks as:

$$(\Delta Y)^2 = \sum_{i=1}^{n} \left(\frac{\partial f}{\partial x_i} \Delta x_i \right)^2 \tag{7.1}$$

Since the total air content value is calculated by:

$$V_{air} = \frac{P_{meas} \cdot V_{ex} \cdot T_s}{M_{ice} \cdot T_{ice} \cdot P_s} \tag{7.2}$$

the error of the calculated value can be calculated as:

$$\frac{\Delta V_{air}}{V_{air}} = \sqrt{\frac{(\Delta V_{ex})^2}{(V_{ex})^2} + \frac{(\Delta P_{meas})^2}{(P_{meas})^2} + \frac{(\Delta M_{ice})^2}{(M_{ice})^2} + \frac{(\Delta T_{meas})^2}{(T_{meas})^2}} \tag{7.3}$$

This gives an overall error of 2.18%. This is the uncertainty of the total air content, but the error of the water trap is not taken into consideration here. This might result in an even larger resultant error. It would probably result in a lower pressure and thereby a lower total air content.

7.1.2   Cut bubble effect

The results are corrected for the cut bubble effect. In Section 5.2 this is determined to be 5.42%, by measuring the size of the bubbles. If the size of the bubbles are underestimated, the cut bubble effect will be underestimated resulting in too low total air content results. The most advantageous shape of an ice sample to decrease the cut bubble effect would be spherical, since this is depending on the surface area

compared to the volume of ice. But this is not preferable for the cutting of the ice samples, so the next best thing is cubic. A factor is found determining how much higher the cut bubble effect is, due to the fact that the samples are not cubic. This means that the cut bubble effect should not be underestimated due to the fact that the samples are not cubic. When the cut bubble effect is calculated, it is assumed that the bubbles are spherical. Though this is a good assumption, it might not be completely correct since cylindrical bubbles might occur, which could increase the effect a bit. The samples in this thesis are small compared to samples used in measurements, where the cut bubble is found to be between 1 and 10%. In Martinerie et al. (1990) the samples have a side length of 3 cm. The relationship between the volume of ice and the surface area is important for the cut bubble effect. This relationship decrease as the size increase. So the fact, that the samples measured in this thesis are smaller compared to other studies, can increase the cut bubble effect. But the size is taken into consideration determining the effect so it can not increase the determined cut bubble effect.

7.2 Comparing the results to results from other studies

The results of the total air content obtained from the experiments of samples from EUROCORE ice core is seen in Figure 6.2. The values, also seen in Table 6.1, lie between $0.0835 - 0.0922\frac{\text{cm}^3}{\text{g}}$ with an error of 2.18% and has a mean value of $0.0881\frac{\text{cm}^3}{\text{g}}$. The results are a bit low compared to the estimated $0.0926\frac{\text{cm}^3}{\text{g}}$, however for the highest results the estimated value lies within the range of the error. In this estimate pore volume, V_c, is determined from the linear regression Equations 2.9, obtained from Figure 2.2, where the pore volume only depends in the temperature. This is a simplification since the pore volume also depend on other parameters like solar insolation. This might explain why the measured total air content value is so much smaller than the estimated value.

In Figure 7.2 the total air content versus elevation from different sites are seen. The red star represents the mean value of the results of total air content obtained in this thesis. It is seen that this value is a bit low compared to the other values from GRIP. Since EUROCORE and GRIP are only 50 m apart the conditions for the two cores are the same, and the total air content in the two cores should be the same. Raynaud et al. (1997) has measured the total air content in the GRIP ice core. These measurements are seen in Figure 1.4. The samples measured in this thesis are from 280 m depth. This correspond to the very first part of the record, where the value of the total air content in GRIP ice core (found by Raynaud et al. (1997)) is around $0.09\frac{\text{cm}^3}{\text{g}}$. This also indicates that the values obtained in this
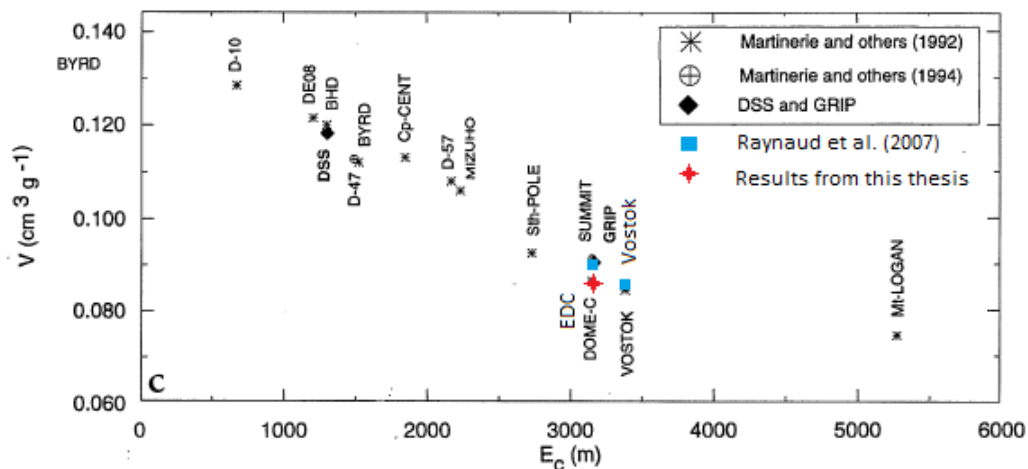
Figure 7.2: Air content versus elevation at close-off E_c. Crosses are adapted from Martinerie et al. (1992) and circles from Martinerie et al. (1994). The diamonds correspond to GRIP (Raynaud et al., 1997) and DSS from Delmotte et al., 1999, which are added by [Delmotte et al., 1999]. Blue squares correspond to results from two sites presented in Raynaud et al., 2007 from EDC (their own) and Vostok from Lipenkov et al., 1997. Modified from [Delmotte et al., 1999]. The red star represent the mean value of the results obtained in this thesis.

thesis are a bit low. It is not clear why they are low. However it is not much lower, and the samples measured in this thesis are taken from a small range of depth so it could be that this small range has a low total air content. The cut bubble effect might be too low but it would have to be 8% to raise the value to a result similar to that obtained by Raynaud et al. (1997). The resultant error of the result of the total air content is 2.18%. This is twice as high as the error Lipenkov et al. (1995) determines (1%) for an experiment that is, in many ways, similar to this experiment. This might be due to larger uncertainties of the the pressure calibration, the volume calibration and the temperature.

The results seem to show seasonal variations, that fit with the variations seen in the $\delta^{18}O$ record from the same depth. The variation have changes of $6.6-8.5\%$. These variations were expected since parameters like accumulation, temperature and insolation influence the density, which can result in annual changes in the pore volume. As it is seen in Figure 1.6 these seasonal variations are also registered in other studies.

7.3 Future improvements of the setup

Three of the parameters that are used to calculate the total air content had to be calibrated: the pressure, the volume and the temperature sensors. The two first were calibrated in the work of this thesis, but the temperature sensors were not calibrated, since it was realized too late that the existing calibrations were invalid. To improve the system further, it would therefore be good to have precise calibrations of the pt1000 temperature sensors. The most important pt1000 sensor is the one placed on the pressure gauge measuring the temperature of the measuring area. It is only necessary to calibrate this sensor in the range of room temperatures. It might be preferable to measure more than one temperature on the measuring area to obtain a more precise measurement, but also to have an extra measurement if something should go wrong.

Furthermore, it would be nice to get rid of the problem with the water trap. Either the error of the water trap would have to be determined making it possible to subtract this error from the measured pressure, or it might be necessary to install a new trap to see if this would remove the problem. If the problem still occurs after changing the water trap, the problem might be due to something that has not been considered.

To verify the determination of the cut bubble effect, it would be good to try to determine the cut bubble effect experimentally. This could be done by measuring samples from the same depth but with different surface areas. If for example the relationship between the surface area and the volume of the sample was doubled, the cut bubble effect would be expected to be doubled. If it was possible to get more than two samples from the same depth, the measured total air content could be plotted against the relationship between the surface area and the volume, and the slope would determine the cut bubble effect.

A great disadvantage of the experiment is that the duration of an experiment is long, and as it is now it is only possible to measure one sample in one day. Having another usable extraction chamber might make it possible to measure two samples in one day. If it was possible to modify the extraction chamber with sides made of plastic so the leak rate of this box was minimized, this extraction chamber could be used instead of the aluminium chamber. If the plastic chamber works optimally, the sample only freezes from the bottom producing ice without air in the first melting/refreezing cycle. This could have the result that only one melting/refreezing cycle is necessary to extract all the air from the sample, which would almost halve the time duration of the experiment. Another approach to be able to measure more sample could be to expand the setup and make it possible to measure more than one sample at the time. This might be possible if several extraction chambers could be connected to the system at the same time.

Chapter 8

Conclusion

The experimental setup build by Bender (2012) to measure the total air content of ice samples, has been expanded by adding a water trap and an air trap so it becomes possible to perform several melting/refreezing cycles and trapping the air between the cycles.

The reason for adding the water trap was to dry the air before it is trapped. This should also decrease the water vapor pressure to be so low that it is not measurable and can be neglected. Unfortunately the trap does not work optimally which results in a small error of the pressure that can not be corrected for.

The air, trap built as a filter filled with HayeSep, works as expected: it traps the air when it is cooled to $-198°$C with liquid nitrogen, and releases the air when it is heated with a water bath with a temperature between $50-80°$C. The capacity of the HayeSep in the trap is 111.45cm^3, which is much higher than the volume of air in the samples. The installation of the air trap in the setup has some nice advantages. The volume of the measuring area no longer changes size due to the size of the sample, because the extraction chamber containing the sample is no longer a part of the measuring area. Since the extraction chamber is no longer a part of the measuring area, the temperature gradient between the chamber ($-30°$C to $-25°$C) and the pressure gauge (room temperature) is no longer present. This simplifies the calculations, and it only becomes necessary to measure one temperature: the temperature of the measuring area.

From experiments with three, four and seven melting/refreezing cycles it was clarified that the majority of the air is released in the first cycle and only two cycles are necessary for all the air to be extracted from the sample. The resultant pressures after the third cycle and upwards is the leak rate. From these resultant pressures the leak rate is determined to be $1.58\frac{\text{Pa}}{\text{h}}$.

The experimental time has been shortened so two melting/refreezing cycles can be performed in 4-5 hours, which halves the time of the previous experiment. This is primarily because the refreezing process is shortened, since it is no longer

necessary to reach a stable temperature as low as possible. It is now only necessary to make sure that the whole sample is completely melted. However it is still only possible to measure one sample per day, because only one extraction chamber is available.

The pressure measurements are very precise, with an accuracy below the precision of 1 Pa. But the calibrated pressure has an uncertainty of ±8.89. This results in an uncertainty of 1.56% of the calibrated pressures between 514-593 Pa. The volume of the measuring area has been calibrated to be 159.39cm^3 with an uncertainty of ±2.36cm^3 resulting in an error of the measuring area volume of 1.44%. The error of the mass is very small and is estimated to be 0.11%. The temperature sensors have not been recalibrated, and the calibration done by Bender (2012) is not valid because the temperatures are too high due to internal heating during the calibration experiment. The temperatures are calculated with the standard Callendar-Von Dusen equations, although doing this is not completely valid. But since these temperatures only differ 1°C from the temperatures registered from the PID, the use of this equation is justified. Still the temperature of the measuring area is not very precise, but a change in the temperature of 1°C will only change result of the total air content 0.3%. The uncertainty is estimated to be ±1°C resulting in an error of 0.34%. From these errors the total error of the total air content measurement is calculated to be 2.18%

The cut bubble effect of the samples is determined to be 5.42%. Determining this it is taken into account that the samples are not cubic, but it is assumed that the bubbles are spherical which might underestimate the cut bubble effect a bit. The measurement of the diameter of the bubbles might also be too low resulting in an underestimated cut bubble effect.

The samples that are measured are from EUROCORE. The resulting values of the total air content obtained from the measurements lie between $0.0835 - 0.0922\frac{\text{cm}^3}{\text{g}}$ and has a mean value of $0.0881\frac{\text{cm}^3}{\text{g}}$. This is low compared to the expected value of $0.0926\frac{\text{cm}^3}{\text{g}}$ found from drill site parameters. This expected value might be too high because the pore volume determined from the temperature is overestimated. The results also show seasonal variations that fit the variations of the $\delta^{18}O$ record from the same depth. This is in accordance with expectations and results from other studies.

All in all it can be concluded that the experiment is working. The expansion with an air trap is successful and has some great advantages. The water trap is not working optimally. The resultant error of the total air content measurements is 2.18%. The results are close to results obtained in other studies from the same site, and they show expected seasonal variations. Though there is still further work that can be done to improve the experimental setup.
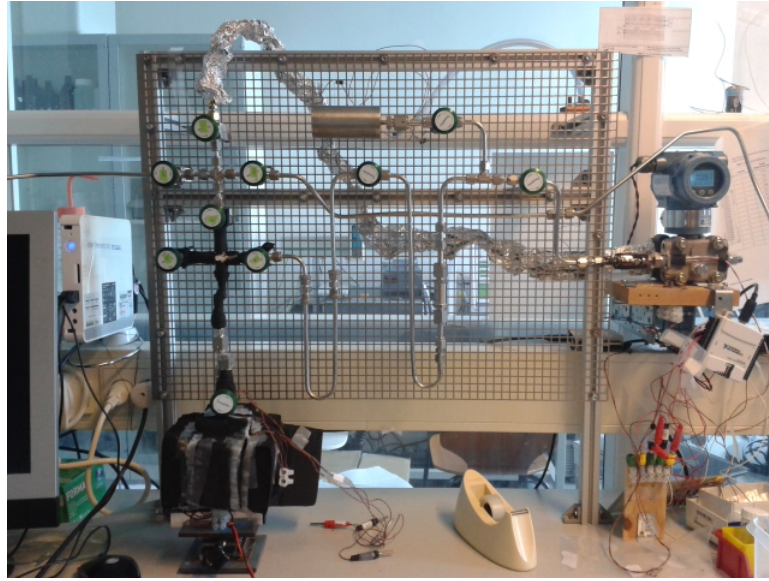
Appendix A
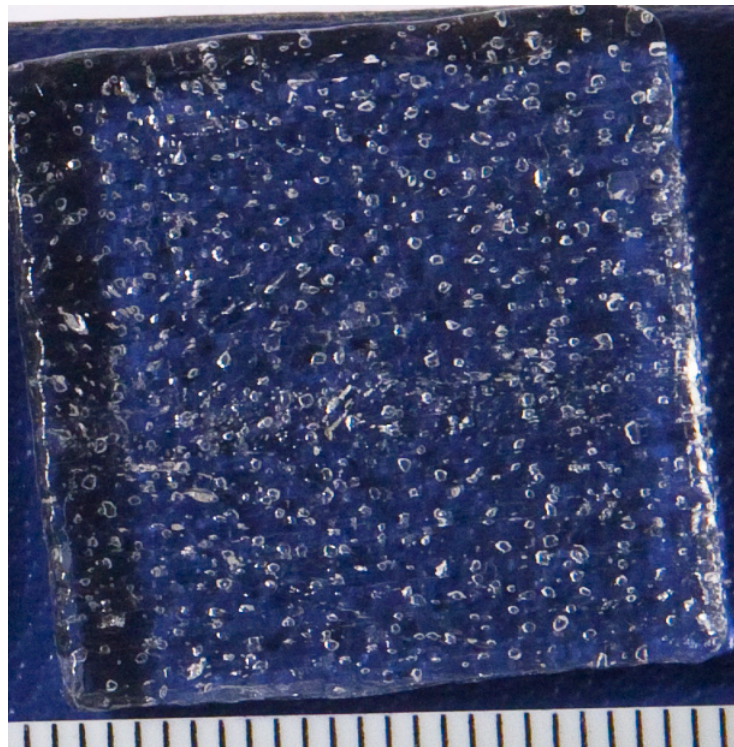
Pictures

Here some pictures that are taken of the experimental setup is shown. First a picture of the previous experimental setup. Then a picture of the new improved experimental setup. Then, some of the close up pictures that were taken if thin slices of ice to determine the cut bubble effect, are seen.
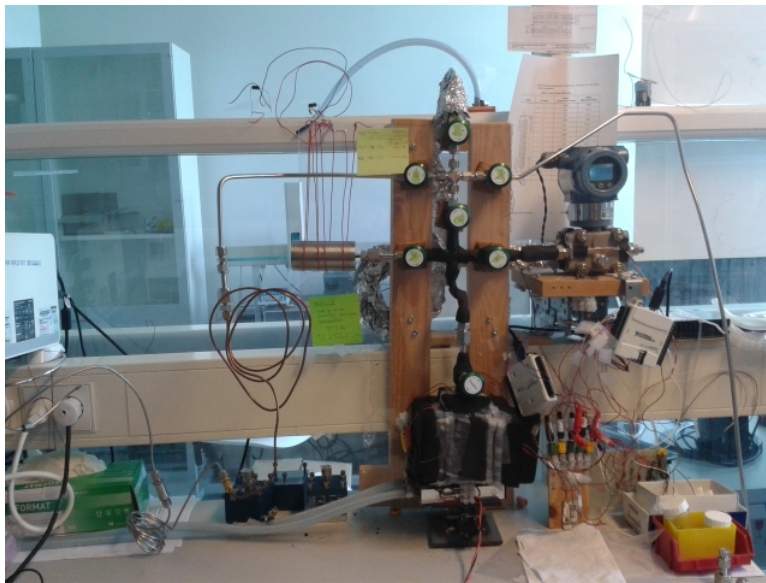
Figure A.1: Picture of the previous experimental setup built by Bender (2012).

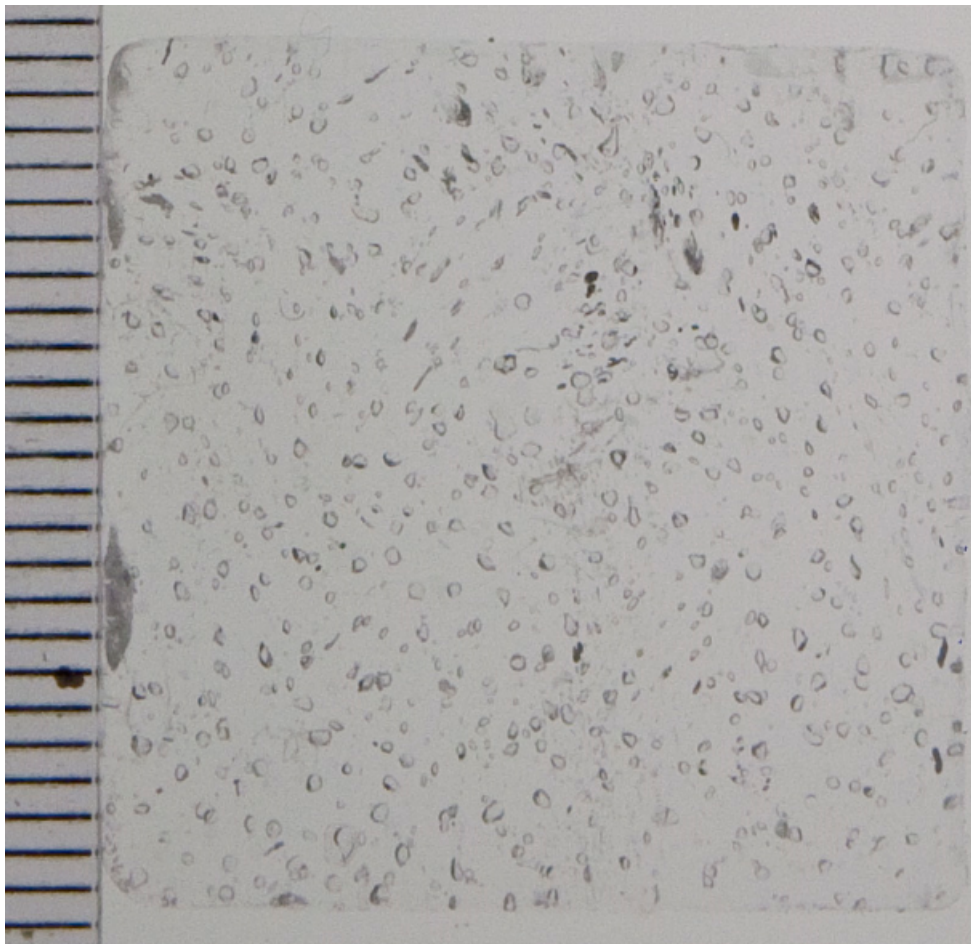**Figure A.2:** Picture of the new, expanded experimental setup.

Figure A.3: Close up picture of a thin slice of ice where the bubbles are seen clearly.

Figure A.4: Close up picture of a thin slice of ice where the bubbles are seen clearly.

Appendix B

Fix resistors

Table of the resistance of the fix resistors built into the Wheatstone bridges. These are measures and determined by Bender (2012).

Resistor	Resistance (Ω)	Sensor	Function
1	91.63	pt100	Wheatstone fix 1
			(highest sensitivity near $-30°C$)
2	110.57	pt100	Wheatstone fix 1
			(highest sensitivity near $25°C$)
3	100.17	pt100	Wheatstone fix 2
4	100.47	pt100	Wheatstone fix 3
5	872.4	pt1	Wheatstone fix 1
6	871.2	pt2	Wheatstone fix 1
7	1085.0	pt3	Wheatstone fix 1
8	1082.4	pt4	Wheatstone fix 1
9	1000.14	pt1	Wheatstone fix 2
10	998.2	pt1	Wheatstone fix 3
11	998.2	pt2	Wheatstone fix 2
12	1009.3	pt2	Wheatstone fix 3
13	1001.0	pt3	Wheatstone fix 2
14	999.4	pt3	Wheatstone fix 3
15	1002.7	pt4	Wheatstone fix 2
16	1003.1	pt4	Wheatstone fix 3
17	100.7	power supply	Measure voltage across
			this R to calculate emf
18	1000.3	power supply	Resistor divide - $R = R17 + R18$
19	39.59	pressure gauge	Divide of load resistance.
			Voltage across this R is measured
20	209.89	pressure gauge	Divide of load resistance
			(load=$R19 + R20$)
			(no measurements on R20)

Table B.1: Table of the resistances of the fix resistors in the Wheatstone bridges.

Appendix C

Pt1000 Temperature sensor calibration equations

To calculate the temperatures from the resistances of the pt1000 temperature sensors, R_T, the sensors have to be calibrated which was done by Bender (2012). The following relations between R_T and the temperatures for the three relevant sensors in experimental setup described in Chapter 3 are found by Bender (2012). The first two are five interval linear and quadratic equation obtained for the two pt1000 temperature sensors placed on the extraction chamber.

$$T_{pt1} = \begin{cases} \dfrac{R_{T1} - 959.7}{3.171} & \text{for} R_{T1} < 869.3\,\Omega \\[2ex] \dfrac{4.622 + \sqrt{21.3629 - 0.0757 * (985.7 - R_{T1})}}{0.0378} & \text{for} R_{T1} \in [869.3\,\Omega; 946.1\,\Omega] \\[2ex] \dfrac{R_{T1} - 982.1}{4.048} & \text{for} R_{T1} \in [946.1\,\Omega; 955.8\,\Omega] \\[2ex] \dfrac{4.622 + \sqrt{17.698 - 0.0243 * (983.4 - R_{T1})}}{0.0122} & \text{for} R_{T1} \in [955.8\,\Omega; 1089.9\,\Omega] \\[2ex] \dfrac{R_{T1} - 997.7}{3.504} & \text{for} R_{T1} > 1089.9\,\Omega \end{cases}$$

and

$$T_{pt2} = \begin{cases} \dfrac{R_{T2} - 954.3}{3.153} & \text{for} R_{T2} < 880.2\,\Omega \\[2ex] \dfrac{4.119 + \sqrt{16.9662 - 2.61 * 10^{-4} * (977.0 - R_{T2})}}{1.3050 * 10^{-4}} & \text{for} R_{T2} \in [880.2\,\Omega; 947.8\,\Omega] \\[2ex] \dfrac{R_{T2} - 976.3}{4.021} & \text{for} R_{T2} \in [947.8\,\Omega; 950.2\,\Omega] \\[2ex] \dfrac{4.159 + \sqrt{17.2973 - 0.0103 * (977.3 - R_{T2})}}{0.0122} & \text{for} R_{T2} \in [950.2\,\Omega; 1086.1\,\Omega] \\[2ex] \dfrac{R_{T2} - 984.6}{3.816} & \text{for} R_{T2} > 1086.1\,\Omega \end{cases}$$

The pt1000 sensor on the measurement area (pt4) does not experience the same temperature changes as the two first pt1000 sensors but is always at room temperature. This sensor is therefore only calibrated in the range of room temperature and the following equation is obtained:

$$T_{pt4} = \frac{R_4}{992.7 - 1} * \frac{1000}{3.71714} \tag{C.1}$$

Bibliography

[Bender, 2012] Sebastian Bender, Master Thesis, 2012. Measurement of air content in the Greenland ice sheet.

[Cuffey and Paterson, 2010] Cuffey, K.M. and Paterson, W.S.B. (2010). *The Physics of Glaciers*. Fourth Edition. Academic press, Boston.

[Delmotte et al., 1999] Delmotte, M., D. Raynaud, V. Morgan, J. Jouzel (1999). Climatic and glaciological information inferred from air-content measurements of Law Dome (East Antarctica) ice core, *Journal of Glaciology*, 45(150), 255-263

[Haan et al., 1996] Haan, D., P. Martinerie and D. Raynaud (1996). Ice core data of atmospheric carbon monoxide over Antarctica and Greenland during the last 200 years, *Geophysical research letters*, 23(17), 2235-2238

[Haynes, W.M., 2014] Haynes, W.M. (Editor-in-chief), (2014). *Handbook of Chemestry and Physics*. 95^{Th} Edition.

[Krinner et al. 2000] Krinner, g., D. Raynaud, C. Doutriaux and H. Dang (2000). Simulations of the Last Glacial Maximum ice sheet surface climate: Implications for the interpretation of ice core air content, *Journal of Geophysical Research*, 105(D2), 2059–2070

[Lipenkov et al. 1995] Lipenkov, V., F. Candaudap, J. Ravoire, E. Dulac and D. Raynaud (1995). Instruments and Methods. Anew device for the measurement of air content in polar ice, *Journal of Glaciology*, 41(138), 423-429

[Martinerie et al., 1990] Martinerie, P., V.Y Lipenkov and D. Raynaud, (1990). Correction of air-content measurements in polar ice for the effect of cut bubbles at the surface of the sample, *Journal of Glaciology*, 36(124), 299-303.

[Martinerie et al., 1992] Martinerie, P., D. Raynaud, D.M. Etheridge, J-M. Barnola and D. Mazaudier, (1992). Physical and climatic parameters which influence the sir content in polar ice, *Earth and Planetary Science Letters*, 112(1992),1-13

[Martinerie et al., 1994] Martinerie, P., V.Y Lipenkov, D. Raynaud, J. Chappellaz, N.I. Barkov and C. Lorius , (1994). Air content paleo record in the Vostoc ice core (Antarctica): A mixed record of climate and glaciological parameters, *Journal of Geophysical research*, 99(D5), 10565-10576.

[North Greenland Ice Core Project members, 2004] North Greenland Ice Core Project members: K. K. Andersen, N. Azuma, J.-M. Barnola, M. Bigler, P. Biscaye, N. Caillon, J. Chappellaz, H. B. Clausen, D. Dahl-Jensen, H. Fischer, J. Flückiger, D. Fritzsche, Y. Fujii, K. Goto-Azuma, K. Grønvold, N. S. Gundestrup, M. Hansson, C. Huber, C. S. Hvidberg, S. J. Johnsen, U. Jonsell, J. Jouzel, S. Kipfstuhl, A. Landais, M. Leuenberger, R. Lorrain, V. Masson-Delmotte, H. Miller, H. Motoyama, H. Narita, T. Popp, S. O. Rasmussen, D. Raynaud, R. Rothlisberger, U. Ruth, D. Samyn, J. Schwander, H. Shoji, M.-L. Siggard-Andersen, J. P. Steffensen, T. Stocker, A. E. Sveinbjörnsdóttir, A. Svensson, M. Takata, J.-L. Tison, Th. Thorsteinsson, O. Watanabe, F. Wilhelms and J. W. C. White (2004). High-resolution record of Northern Hemisphere climate extending into the last interglacial period, *Nature*, 431, 147-151.

[Raynaud and Lorius, 1973] Raynaud, D and C. Lorius (1973). Climatic implications of total gas content in ice at Camp Century, *Nature*, 243, 283-284.

[Raynaud and Lebel, 1979] Raynaud, D and B. Lebel (1979). Total gas content and surface elevation of polar ice sheets, *Nature*, 281, 289-291.

[Raynaud et al., 1997] Raynaud, D., J. Chappellaz, C. Ritz and P. Martinerie (1997). Air content along the Greenland Ice Core Project core: A record of surface climatic parameters and elevation in central Greenland, *Journal of Geophysical Research*, 102(C12), 26607–26613

[Raynaud et al., 2007] Raynaud, D., V. Lipenkov, B. Lemieux-Dudon, P. Duval, M-F. Loutre and N. Lhomme (2007). The local insolation signature of air content in the Antarctic ice. A new step toward an absolute dating of ice records, *Earth and Planetary Science Letters*, 261(2007), 337-349

[Schwander et al., 1997] Schwander, J., T. Sowers, J.-M. Barnola, T. Blunier, A. Fuchs and B. Malaizé (1997). Age scale of the air in the summit ice: Implication for glacial-interglacial temperature change, *Journal of Geophysical Research*, 102(D16), 19483-19493

[Taylor, 1997] Taylor, John R., (1997). *An introduction to Error Analysis*. Second Edition. University Science Books, Sausalito, California.

[Vagle and Farmer, 1998] Vagle, S. and D. M. Farmer (1998). A Comparison of Four Methods for Bubble Size and Void Fraction Measurements, *Journal of oceanic engineering*, 23(3), 211-222

[Vazquez et al., 2005] Vazquez, A., R.M. Sanchez, E. Salinas-Rodriguez, A. Soria and A. Manasseh (2005). A look at three measurement techniques for bubble size determination, *Experimental Thermal and Fluid Science*, 30(2005), 49-57

[Vinther et al., 2009] Vinther, B.M., S.L. Buchardt, H.B. Clausen, D. Dahl-Jensen, S.J.Johnson, D.A. Fisher, R.M. Koerner, D. Raynaud, V. Lipenkov, K.K. Andersen, T. Blunier, S.O. Rasmussen, J.P. Steffensen and A.M. Svensson (2009). Holocene thinning of the Greenland ice sheet, *Nature*, 461, 385-388.

[Swagelok Filter catalogue, 2014] Swagelok (2014). FW, F, and TF Series, Filters, `http://www.swagelok.com/downloads/webcatalogs/en/ms-01-92.pdf`, Accessed: December, 2014.

[Operation Instructions; Rotary Vane Pump, 2014] Pfeiffer Vacuum, (2014). Operation Instructions; Rotary Vane Pump, UNO/DUO 2.5, DUO 2.5 CUNO 5, `http://conquerscientific.com/wp-content/ad_images/Pfeiffer-Duo-2.5-Vacuum-Pump.pdf`, Accessed: November, 2014.

[Vici, HayeSep porouos polymers (2014)] Vici; HayeSep porouos polymers, `http://www.vici.com/hayesep/hayesep.php`, Accessed: November, 2014.

[Pressure Gauge Manual, 2014] SGM Lektra (2014). P-BADP / P-BADR, Smart/HART pressure transmitter, `file:///C:/Users/ejer/Downloads/PBA\%20(1).pdf` Accessed: December, 2014.

[Digiquartz Portable Standard Manual, 2014] Paroscientific, Inc., (2014). Portable Pressure Standard, Model 760, `http://www.paroscientific.com/pdf/Model760.pdf` Accessed: December, 2014.